

## BASIC SCIENCES

# Circadian Dysfunction in the Skeletal Muscle Impairs Limb Perfusion and Muscle Regeneration in Peripheral Artery Disease

Pei Zhu (朱培)<sup>1</sup>, Calvin L. Chao, Adam W.T. Steffek<sup>1</sup>, Caitlyn Dang<sup>1</sup>, Noah X. Hamlish<sup>1</sup>, Eric M. Pfrender, Bin Jiang<sup>1</sup>, Clara B. Peek<sup>1</sup>

**BACKGROUND:** Peripheral artery disease (PAD), caused by atherosclerosis, leads to limb ischemia, muscle damage, and impaired mobility in the lower extremities. Recent studies suggest that circadian rhythm disruptions can hinder vascular repair during ischemia, but the specific tissues involved and the impact on muscle health remain unclear. This study investigates the role of the skeletal muscle circadian clock in muscle adaptation to ischemic stress using a surgical mouse model of hindlimb ischemia.

**METHODS:** We performed secondary analysis of publicly available RNA-sequencing data sets derived from patients with PAD to identify the differential expression of circadian-related genes in endothelial cells and ischemic limb skeletal muscles. We used mice with specific genetic loss of the circadian clock activator, BMAL1 (brain and muscle ARNT-like 1), in adult skeletal muscle tissues (*Bmal1<sup>muscle</sup>*). *Bmal1<sup>muscle</sup>* mice and controls underwent femoral artery ligation surgery to induce hindlimb ischemia. Laser Doppler imaging was used to assess limb perfusion at various time points after the surgery. Muscle tissues were analyzed with RNA sequencing and histological examination to investigate PAD-related muscle pathologies. Additionally, we studied the role of BMAL1 in muscle fiber adaptation to hypoxia using RNA and assay for transposase-accessible chromatin with sequencing analyses in primary myotube culture model.

**RESULTS:** Disrupted expression of circadian rhythm-related genes was observed in existing RNA-sequencing data sets from endothelial cells and ischemic limb skeletal muscles derived from patients with PAD. Genetic loss of *Bmal1* specifically in adult mouse skeletal muscle tissues delayed reperfusion recovery following induction of hindlimb ischemia. Histological examination of muscle tissues showed reduced regenerated myofiber number and a decreased proportion of type IIB fast-twitch myofibers in *Bmal1<sup>muscle</sup>* mouse muscles in the ischemic limbs but not in their contralateral nonischemic limbs. Transcriptomic analysis revealed abrogated metabolic, angiogenic, and myogenic pathways relevant to hypoxia adaptation in *Bmal1<sup>muscle</sup>* mouse muscles. These changes were corroborated in *Bmal1*-deficient cultured primary myotubes cultured under hypoxic conditions.

**CONCLUSIONS:** Circadian clock in skeletal muscle is crucial for the muscle's response to hypoxia during hindlimb ischemia. Targeting the muscle circadian clock may have therapeutic potential for enhancing muscle response to reduced blood flow and promoting recovery in conditions such as PAD.

**GRAPHIC ABSTRACT:** A graphic abstract is available for this article.

**Key Words:** circadian clocks ■ femoral artery ■ ischemia ■ peripheral artery disease ■ reperfusion

Peripheral artery disease (PAD) represents a significant health burden globally, characterized by the narrowing or blockage of arteries supplying blood to

the lower extremities.<sup>1</sup> One of the prominent manifestations of PAD is lower extremity skeletal muscle pathology, including reduced muscle area, increased fatty

Correspondence to: Bin Jiang, PhD, Northwestern University Feinberg School of Medicine, 303 E Superior St, SQ11-526, Chicago, IL 60611, Email bin.jiang@northwestern.edu; or Clara B. Peek, PhD, Northwestern University Feinberg School of Medicine, 303 E Superior St, SQ7-408, Chicago, IL 60611, Email c-peek@northwestern.edu

Supplemental Material is available at <https://www.ahajournals.org/doi/suppl/10.1161/ATVBAHA.124.321772>.

For Sources of Funding and Disclosures, see page e45.

© 2024 American Heart Association, Inc.

*Arterioscler Thromb Vasc Biol* is available at [www.ahajournals.org/journal/atvb](http://www.ahajournals.org/journal/atvb)

## Nonstandard Abbreviations and Acronyms

|                               |                                                            |
|-------------------------------|------------------------------------------------------------|
| <b>ATAC-seq</b>               | assay for transposase-accessible chromatin with sequencing |
| <b>BMAL1</b>                  | brain and muscle ARNT-like 1                               |
| <b>CL</b>                     | control limb                                               |
| <b>CLI</b>                    | critical limb ischemia                                     |
| <b>DAPI</b>                   | 4',6-diamidino-2-phenylindole                              |
| <b>DEG</b>                    | differentially expressed gene                              |
| <b>EC</b>                     | endothelial cell                                           |
| <b>HIF</b>                    | hypoxia-inducible factor                                   |
| <b>HLI</b>                    | hindlimb ischemia                                          |
| <b>HRP</b>                    | horseradish peroxidase                                     |
| <b>iPSC</b>                   | induced pluripotent stem cell                              |
| <b>LDI</b>                    | laser Doppler imaging                                      |
| <b>MEF2</b>                   | myocyte enhancer factor 2                                  |
| <b>MSTN</b>                   | myostatin                                                  |
| <b>PAD</b>                    | peripheral artery disease                                  |
| <b>PCR</b>                    | polymerase chain reaction                                  |
| <b>PDGF</b>                   | platelet-derived growth factor                             |
| <b>PER2</b>                   | Period 2                                                   |
| <b>RNA-seq</b>                | RNA sequencing                                             |
| <b>TA</b>                     | tibialis anterior                                          |
| <b>TGF-<math>\beta</math></b> | transforming growth factor- $\beta$                        |
| <b>VEGFA</b>                  | vascular endothelial growth factor- $\alpha$               |

infiltration, fibrosis, and metabolic abnormalities, leading to impaired walking performance and loss of mobility.<sup>2</sup> Despite advances in diagnostic techniques and therapeutic interventions, such as revascularization procedures, many patients with PAD continue to experience limited efficacy and adverse outcomes. The interplay between vascular insufficiency and skeletal muscle dysfunction underscores the need for a deeper understanding of the underlying mechanisms driving pathological changes in PAD. Furthermore, the identification of novel therapeutic targets is imperative to address the unmet clinical need for effective interventions that can improve limb perfusion, muscle health, and overall functional outcomes in individuals with PAD.

Many traditional risk factors of PAD, including advanced age, diabetes, and cigarette smoking, are associated with disrupted circadian clock function.<sup>3</sup> Additionally, patients with chronic limb-threatening ischemia, the most severe form of PAD, are often plagued by nocturnal ischemic rest pain and other clock-disrupting comorbidities, such as obstructive sleep apnea.<sup>4,5</sup> Mammalian circadian clocks are cell-autonomous networks that coordinate behavior and metabolism with the rotation of the Earth.<sup>3</sup> The master pacemaker neurons in the brain are entrained, or reset, primarily by light, while peripheral clocks are entrained by both signals from the master pacemaker and by nutrient

## Highlights

- Endothelial cells and ischemic limb skeletal muscles derived from a patient with PAD exhibit disrupted expression of circadian rhythm-related genes.
- The skeletal muscle molecular clock is required for normal reperfusion and myofiber regeneration in ischemic mouse limbs following femoral artery ligation.
- The muscle molecular clock directs hypoxia-adaptive gene networks involved in HIF-dependent metabolism and angiogenesis.
- Muscle loss of the clock activator *Bmal1* results in larger regenerated myofibers with reduced proportion of type 2b fibers, possibly due to altered MEF2a and MyoD activity.

availability.<sup>6</sup> Peripheral clocks are present throughout the body, including vascular and skeletal muscle tissues. At the cellular level, the clock network controls expression of thousands of genes to align cell-specific processes and metabolism with the changing demands across the 24-hour day. The molecular clock network consists of an autoregulatory transcription-translation feedback loop in which the basic helix-loop-helix/Per-ARNT-SIM (bHLH-PAS) domain-containing transcription factor activators (CLOCK [circadian locomotor output cycles kaput]/BMAL1 [brain and muscle ARNT-like 1]) induce the expression of repressors (PER [period]/CRY [cryptochrome]) that feed back to inhibit the activators in a cycle that repeats itself every  $\approx$ 24 hours.<sup>7</sup> Individuals exposed to shiftwork, sleep loss, or jet lag experience both conflicts between environmental and internal rhythms and desynchrony among brain and peripheral clocks, which leads to increased susceptibility to metabolic diseases. Disruptions to circadian rhythms have been implicated in exacerbating vascular endothelial dysfunction, impairing skeletal muscle metabolism, and compromising the regenerative capacity of tissues.<sup>8–13</sup> Despite this emerging understanding, the precise mechanisms linking circadian disruption to PAD-associated vascular and muscle pathology remain incompletely understood.

We previously discovered a novel bidirectional connection between the circadian activator BMAL1 and the related factor HIF (hypoxia-inducible factor) 1A.<sup>14</sup> We observed that this interaction allows the circadian clock to regulate HIF responses throughout the day, influencing how muscle responds to low oxygen levels during exercise<sup>14</sup> and acute myotoxin injury.<sup>13</sup> Given the presence of hypoxia and HIF pathway<sup>15,16</sup> activation in ischemic muscle tissues, we posited that the adaptation to low oxygen levels in ischemic limbs during PAD may be influenced by the circadian clock. In this study, we hypothesized that circadian disruption in the skeletal muscle underlies the progression and severity of ischemia in patients with

PAD. In support of this, using previously published human clinical study data sets, we observed dysregulation of circadian networks in patients with PAD. Furthermore, we found that genetic circadian clock disruption specifically in adult mouse skeletal muscle tissues leads to delayed reperfusion repair and reduced myofiber size following surgical induction of hindlimb ischemia (HLI). Molecular characterization of clock-deficient muscles following surgery revealed abrogated metabolic, angiogenic, and myogenic pathways relevant to hypoxia adaptation. Together, this study implicates the muscle autonomous circadian clock in the adaptation and recovery from HLI, raising the potential for future targeting of circadian networks to combat PAD-related muscle pathologies.

## MATERIALS AND METHODS

To follow the Transparency and Openness Promotion guidelines, all data supporting the findings of this study are available from the corresponding author upon reasonable request. RNA-sequencing (RNA-seq) data from the skeletal muscle tissue in vivo and cultured myotubes are available in the Gene Expression Omnibus under accession codes GSE275811 and GSE275812. Assay for transposase-accessible chromatin with sequencing (ATAC-seq) data from cultured myotubes are available in the Gene Expression Omnibus under accession code GSE275893.

### PAD Patient Data Set Extraction and Analysis

Previously published human transcriptomics data sets GSE236430<sup>17</sup> and GSE120642<sup>18</sup> were obtained from the Gene Expression Omnibus repository. These data sets were used to compare clock-controlled gene expression pattern between patients with PAD and healthy subjects. In data set GSE236430, peripheral blood mononuclear cells from patients and healthy individuals were reprogrammed into induced pluripotent stem cells (iPSCs), followed by directed differentiation into endothelial cells (ECs) under xeno-free conditions. RNA-seq was performed on these iPSC-derived ECs. Detailed information on the human subjects used for generating the iPSC-derived ECs is provided in Table S2, adapted from the original study.<sup>17</sup> For data analysis, raw fastq files were downloaded and processed as described in RNA-seq and Analysis. The normalized count table generated using DESeq2 was subjected to gene set enrichment analysis with the GSEA software (v4.2.2)<sup>19,20</sup> from the Broad Institute. Gene sets from the Molecular Signatures Database, including the Hallmark, Gene Ontology Biological Processes, and WikiPathways collections, were used as references. Enrichment scores were calculated using 1000 permutations of the gene sets, and a false discovery rate  $q$  value of  $<0.25$  was considered significant.<sup>20,21</sup> In data set GSE120642, RNA-seq was performed on gastrocnemius muscle biopsies obtained from 15 healthy older adults and 16 patients with critical limb ischemia (CLI) undergoing limb amputation. Information on the healthy individuals and those with CLI is provided in Table S2, adapted from the original study.<sup>18</sup> For data analysis, the trimmed mean of M values normalized read counts table was downloaded from the Gene Expression Omnibus repository and analyzed using the GSEA software for pathway enrichment, following the same protocol described above.

## Mice

*Bmal1<sup>flx/flx</sup>* mice,<sup>22</sup> provided by Dr Joseph Bass at the Northwestern University, were crossed with ACTA-rtTA-TRE-Cre transgenic mice, provided by Dr Grant Barish at the Northwestern University to produce *Bmal1<sup>flx/flx</sup>;ACTA-rtTA-TRE-Cre* (*Bmal1<sup>muscle</sup>*) mice and *Bmal1<sup>+/+</sup>;ACTA-rtTA-TRE-Cre* littermate controls. To achieve Cre-mediated excision of the flox-flanked sequence, mice received 3 consecutive oral gavages of 200  $\mu$ L doxycycline (10 mg/mL; No. D9891; Sigma) followed by doxycycline-containing drinking water (2 g/L) throughout the experimental duration. The mice were all on a 57BL/6J background and housed under a 12:12 light:dark cycle. All procedures were conducted using male mice aged 3 to 6 months, in strict accordance with the guidelines of the Institutional Animal Care and Use Committee at the Northwestern University. The number of experimental mice specified for each experiment represents the number of biological replicates.

### Induction of HLI

Mice were anesthetized with a continuous flow of 2.0% isoflurane. The skin overlying the right femoral artery was shaved and sharply incised, followed by electrocautery of the underlying inguinal fat pad. The femoral artery was carefully dissected free from the femoral vein and nerve. To induce HLI, a double-knot approach was utilized to ligate the femoral artery proximally with 7-0 silk suture (Teleflex, Wayne, PA). The femoral artery was then ligated at its distal extent with 7-0 silk suture. Hemostasis was ensured and the overlying skin was closed with 9-mm wound clips (Stoelting, Wood Dale, IL). Reduction in limb perfusion ( $>90\%$ ) was immediately confirmed via laser Doppler imaging (LDI). Postoperatively, meloxicam (10 mg/kg) and buprenorphine ER-Lab (0.6 mg/kg) were administered for analgesia. Mice were continuously monitored postoperatively until they were ambulatory, with respiratory rate and activity visually assessed. They were kept on a warming blanket to maintain body temperature. Once recovered, they were returned to their cages and monitored daily for activity, appearance, food/water intake, signs of distress, infection, and blood flow perfusion. In case of hemorrhage, moderate pressure was applied until bleeding stopped. Any infections were treated after consultation with a veterinarian. Early euthanasia was performed if there was over 20% weight loss, lack of food consumption, significant gangrene, extreme dermatitis, or self-injurious behaviors. If surgical staples were forcibly removed, euthanasia would be conducted via CO<sub>2</sub> asphyxiation and cervical dislocation. Throughout the entire experiment, 1 mouse in the control group died. This was likely secondary to a large right inguinal hernia noted after dissection of the inguinal fat pad, just superior to the site of femoral artery ligation. Due to some unexpected technical issues with our staining for type IIb/IIa fibers, which led to loss of several samples, additional pairs of animals ( $n=4$  control and  $n=5$  *Bmal1<sup>muscle</sup>* mice) that underwent the same experimental procedure as described in Figure 2A were included in the analyses of Figure 3D and Figure S5C.

### Laser Doppler Imaging

Both ischemic and nonischemic limbs were noninvasively evaluated via LDI, utilizing the MoorLDI2 system (Moor Instruments, Wilmington, DE) on postoperative days 0, 1, 8, 15, 22, and 29.

Mice were anesthetized with a continuous flow of 2.0% isoflurane. Mice were placed prone on a warmed surface to maintain a core temperature of 37 °C for 5 minutes before initiation of LDI. Mice were scanned from the mid-abdomen to the distal extent of bilateral hind limbs. To evaluate limb perfusion, the ischemic right limb and nonischemic left limb were circumscribed utilizing the Moor Laser Doppler Imager, version 5.3 (Moor Instruments), to collect mean tissue perfusion units on a scale from 0 to 1000. In animals with significant tissue loss, the initial intact limb area from postoperative day 0 was utilized to normalize subsequent time points. Limb perfusion was then expressed as a ratio of perfusion units in the ischemic right limb versus the nonischemic left limb for each mouse at each time point.

## Histology

To evaluate muscle regeneration, tibialis anterior (TA) muscles from both ischemia-injured limb (HLI) and the contralateral control limb (CL) were harvested at day 36 after the surgery, when myofiber remodeling and maturation are generally completed, and embedded in a thin layer of Tissue-Tek O.C.T. Compound (No. NC9806257; Fisher Scientific). The samples were snap-frozen in liquid nitrogen-chilled isopentane and stored at -80 °C for later processing. Continuous 10- $\mu$ m-thick cross-sections of the frozen TAs were prepared using a Leica CM1860 cryostat. For hematoxylin and eosin staining, sections were air-dried, rehydrated, and fixed in 10% formalin. The nuclei were stained with hematoxylin, and the cytoplasm and connective tissues were stained with eosin sequentially. The dehydrated sections were mounted with Permount mounting medium (No. 100496-552; VWR). For Masson trichrome staining, tissues were brought to room temperature before fixation in 4% paraformaldehyde for 1 hour. Tissues subsequently underwent standard staining procedure for flash-frozen tissue. For oil red O staining, tissues were fixed for 10 minutes and rehydrated before staining with oil red O working solution and counterstaining with hematoxylin. The prepared slides were examined using the Keyence BZ-X800 or Olympus CKX53 microscope. The cross-sectional area of myofibers was quantified using the FIJI software with the LabelsToROIs<sup>23</sup> plugin. Fibrosis and fat infiltration were quantified in FIJI using color deconvolution vectors.<sup>24</sup>

## Immunohistochemistry

Tissue sections were first air-dried for 30 minutes at room temperature. After drying, they were fixed with 4% paraformaldehyde and permeabilized using 0.25% Triton X-100 for 15 minutes. Blocking for nonspecific binding was performed by treating with PBS containing 5% goat serum, 2% BSA, and 1% Tween 20 for 1 hour. Subsequently, the sections were incubated at 4 °C with primary antibodies, including anti-laminin (No. L9393; Sigma; 1:100), anti-MYH2 (No. SC71; Developmental Studies Hybridoma Bank [DSHB]; 1:200), and anti-MYH4 (No. BF-F3; DSHB; 1:200) antibodies in a diluent buffer of PBS with 0.5% goat serum, 2% BSA, and 1% Tween 20. The sections were then washed 3 $\times$  with PBS and incubated with Alexa Fluor-conjugated secondary antibodies at a 1:1000 dilution for 1 hour at room temperature. Finally, the sections were mounted using VectaShield HardSet antifade mounting medium with DAPI (4',6-diamidino-2-phenylindole;

No. H-1500-10; Vector Laboratories) and visualized under the Keyence BZ-X800 microscope.

## Western Blotting

To prepare total protein lysates from gastrocnemius muscles, each snap-frozen muscle specimen was placed in 500  $\mu$ L of CellLytic Mammalian Tissue Lysis Reagent (No. C3228; Sigma) supplemented with protease inhibitors (No. P8340; Sigma) and mechanically homogenized to ensure uniform cell disruption. After homogenization, protein concentrations were determined using the DC Protein Assay Kit (No. 5000111; Bio-Rad), facilitating accurate loading for SDS-PAGE gel electrophoresis. The proteins separated by electrophoresis were then transferred onto 0.45- $\mu$ m nitrocellulose membranes for immunoblotting. Specific proteins were detected by incubating the membranes overnight at 4 °C with primary antibodies, including anti-BMAL1 (No. 14020; Cell Signaling Technology [CST]), MSTN (myostatin; No. ab203076; Abcam), and  $\alpha$ -tubulin (No. 2144; CST). Following primary antibody incubation, the membranes were washed and incubated with appropriate HRP (horseradish peroxidase)-conjugated secondary antibodies. Protein bands were visualized using an enhanced chemiluminescence detection system, enabling quantitative analysis of protein expression levels.

## RNA Extraction and Real-Time Quantitative Polymerase Chain Reaction

RNA was extracted from gastrocnemius muscles and myotubes derived from primary myoblasts using the TRIzol reagent. The quality and integrity of the RNA were assessed with NanoDrop 2000 spectrophotometers, and only RNA samples with an OD 260/280 ratio >1.80 were used for further analysis. First-strand cDNA synthesis was performed using the Applied Biosystems High-Capacity cDNA Reverse Transcription Kit. Real-time quantitative polymerase chain reaction (PCR) was conducted with iTaq Universal SYBR Green Supermix (Bio-Rad) on the CFX Opus 384 Real-Time PCR System. Quantitative PCR data were analyzed using the  $\Delta\Delta$ Ct method for comparisons of mRNA abundance, with gene expression normalized to  $\beta$ -actin. Primer sequences are provided as follows:  $\beta$ -actin, forward: 5'-TTGTCCCCCAACTTGATGT-3';  $\beta$ -actin, reverse: 5'-CCTGGCTGCCTCAACACCT-3'. Mef2a, forward: 5'-ACTCGTGTCACCGTCTTTGGCA-3'; Mef2a, reverse: 5'-GAGGTCTGTAGTGCTCAACATCC-3'. Mef2c, forward: 5'-GTGGTTCCGTAGCAACTCCTAC-3'; Mef2c, reverse: 5'-GGCAGTGTGAAGCCAGACAGA-3'. Mef2d, forward: 5'-GGTTTCCGTGGCAACACCAAGT-3'; Mef2d, reverse: 5'-GCAGGTGAAGCTGAGGTA-3'. Vegfa, forward: 5'-CTGCTGTAACGATGAAGCCCTG-3'; Vegfa, reverse: 5'-GCTGTAGGAAGCTCATCTCTCC-3'. Mstn, forward: 5'-AACCTTCCCAGGACCAGGAGAA-3'; Mstn, reverse: 5'-GGCTTCAAATCGACCGTGAGG-3'; Bmal1, forward: 5'-AGGCCACAGTCAGATTGAA-3'; Bmal1, reverse: 5'-TGGTACCAAAGAAGCCAATTCAT-3'.

## RNA-seq and Analysis

Total RNA from primary myoblast-derived myotubes and snap-frozen mouse TA muscles were isolated using the Direct-zol RNA MicroPrep Kit (Zymo Research). For muscle tissue samples, half of the TA muscle specimen was initially placed in 500  $\mu$ L of Ambion TRIzol Reagent (No. 15596018; Thermo

Scientific) and homogenized using the TissueLyser II apparatus (Qiagen). Total RNA was quantified using the Qubit RNA Broad-Range Assay Kit (No. Q10210; Thermo Fisher), and the quality was evaluated using the Agilent 2100 Bioanalyzer. cDNA libraries were constructed from 1 µg of total RNA using the TruSeq stranded total RNA library preparation kit (Illumina 20020596). DNA fragments in the library were amplified, size-selected using AMPure XP beads (Beckman Coulter A63880) to enrich fragments between 200 and 500 bp. The pooled libraries were sequenced using NovaSeq 6000 SP Reagent Kit v1.5 (100 cycles) on the NovaSeq 6000 system, executing a paired-end run (51 bp, repeated twice) to achieve a sequencing depth of ~50 million reads per sample.

Demultiplexing of raw BCL files into paired-end read FastQ files was performed using the bcl2fastq software (v2.19.1). After removing the adaptor sequences using the Trimmomatic (v0.33) tool,<sup>25</sup> the trimmed reads were mapped to the mm10 *Mus musculus* reference genome using STAR aligner (v2.5.2).<sup>26</sup> The number of alignments mapped to each gene was counted using RSEM (v1.3.3),<sup>27</sup> followed by passing to DESeq2<sup>28</sup> using the tximport package.<sup>29</sup> Differentially expressed genes (DEGs) were identified through the results function in DESeq2 and corrected for multiple testing (an adjusted *P* value was generated using the Benjamini-Hochberg correction). Gene counts for DEGs were visualized using the pheatmap (v1.0.12) and EnhancedVolcano (version 1.2.0) packages in R. The Kyoto Encyclopedia of Genes and Genomes (KEGG) pathway enrichment and gene ontology analyses were performed using EnrichR<sup>30</sup> or ClusterProfiler.<sup>31</sup> De novo motif discovery was performed on DEGs using the HOMER (v4.10)<sup>32</sup> findMotifs.pl program by searching for motifs of lengths 6, 8, and 10 bp from -1000 to +500 bp relative to the transcriptional start site.

## ATAC-seq and Analysis

Sample for ATAC-seq was prepared in a protocol as previously reported.<sup>12</sup> In brief, myotubes grown in 6-well plates were washed with 1× PBS, then scraped and collected into 1.5-mL Eppendorf LoBind tubes via centrifugation at 500g for 5 minutes at 4 °C. The cells were then permeabilized in 50 µL of a detergent-enhanced assay for transposase-accessible chromatin buffer (10 mmol/L Tris-HCl pH 7.4, 10 mmol/L NaCl, 3 mmol/L MgCl<sub>2</sub>, 0.1% IGEPAL (octylphenoxypolyethoxyethanol), 0.1% Tween 20, and 0.01% digitonin) and incubated on ice for 3 minutes. Subsequently, 1 mL of ice-cold resuspension buffer with Tween 20 (10 mmol/L Tris-HCl, 10 mmol/L NaCl, 3 mmol/L MgCl<sub>2</sub>, and 0.1% Tween 20) was added, and the tubes were inverted to mix. The cell suspension was passed through a BD insulin needle once to ensure complete lysis and nuclear release. The nuclear suspension was then counted using a hemocytometer, and ~50 000 nuclei were transferred to a new LoBind tube and pelleted by centrifugation at 500g for 10 minutes at 4 °C. The supernatant was carefully removed, and the nuclear pellet was resuspended in 50 µL of transposition mix (Illumina Tagment DNA Enzyme and Buffer small kit 20034197) containing 0.01% digitonin and 0.1% Tween 20. The mixture was incubated at 37 °C for 30 minutes in a thermomixer with shaking at 1000 rpm. Tagmented DNA was purified using the MinElute Qiagen Cleanup Kit (Qiagen 28206) and amplified via PCR using NEBNext high-fidelity 2× PCR master mix (NEB M0541). The libraries were size-selected

with Pippin Prep (2% gel cassette for 100- to 600-bp fragments) and purified with AMPure XP beads (Beckman Coulter A63880). Each library was quantified using the NEBNext Library Quant Kit (NEB E7630), then pooled and sequenced on Illumina NextSeq 500 using paired-end runs (51 bp each) to achieve a depth of ~30 million reads per sample.

For data analysis, the paired-end FastQ files were concatenated and the trimmed reads were aligned to the mm10 *Mus musculus* reference genome using Bowtie2 (v2.4.1)<sup>33</sup> with the default settings, except for the -very-sensitive option. The aligned reads were then sequentially filtered to remove mitochondrial DNA using SAMtools (v1.10.1), PCR duplicates with Picard MarkDuplicates program, and nonunique alignments with a mapping quality score <30 using SAMtools (v1.10.1). Peak calling was performed using MACS2 with the parameters -f BAMPE -g mm -keep-dup all. The ENCODE blacklist regions were excluded from the called peaks using the BEDtools (v2.29.2) intersect function. Differential accessibility analysis followed the workflow provided in a previous study.<sup>34</sup> The identified sites of differential chromatin accessibility were annotated using the HOMER (v4.10) annotatePeaks.pl program. The ATAC-seq signal heatmap was generated based on the global peak-centered regions across all conditions. For signal coverage calculation, the Binary Alignment Map (BAM) files, containing aligned ATAC-seq reads, were converted to bigWig files using bamCoverage from the deepTools suite,<sup>35</sup> ensuring normalization across samples. The signal coverage around the peak centers was then calculated using the computeMatrix tool, with the reference point set to the peak center and extending 2 kb upstream and downstream. The computed matrix of signal intensities was visualized as a heatmap using plotHeatmap. The heatmap was centered on the peak summits and overlaid with an average signal profile to highlight trends in the chromatin accessibility pattern between wild-type and *Bmal1*-deficient myotubes under normoxia and hypoxia conditions.

## ELISA

The concentration of VEGFA (vascular endothelial growth factor- $\alpha$ ) released by myotubes into the culture medium was quantified using the Mouse VEGF ELISA Kit (No. MMV00-1; R&D Systems) following the instructions provided by the manufacturer.

## Gene Knockdown

The validated pLKO.1 plasmids containing predesigned shRNAs of Mef2a (TRCN0000095961 and TRCN0000095959), Mef2c (TRCN0000012072 and TRCN0000012069), and Mef2d (TRCN0000315949 and TRCN0000085268) were purchased from Millipore Sigma. The pLKO.1 control shRNA plasmid (containing nontarget scramble shRNA, Addgene plasmid No. 1864<sup>36</sup>) was purchased from Addgene. To generate lentiviruses, the packaging plasmids cocktail containing pCMV-VSVG and psPAX2 was cotransfected with individual pLKO.1-shRNA into 293T cells. The viral supernatant was collected from 48 to 96 hours post-transfection and incubated with primary myoblast-derived myotubes in the presence of 8 µg/mL polybrene (Sigma). Successful infection of the myotubes was confirmed by detecting GFP (green fluorescent protein) fluorescence under a microscope.

## Statistical Analysis

Statistical analysis was performed using GraphPad Prims 10 (GraphPad Software, Inc). Data were expressed as mean±SEM. Normality and homogeneity of variances were tested using the Shapiro-Wilk test and *F* test, respectively, in GraphPad Prism. When both assumptions (normality and equal variances) were met, parametric tests such as ANOVA (for groups >2) or the standard *t* test (for groups =2) were applied. If the *F* test indicated a significant difference in variances ( $P<0.05$ ), Welch *t* test, which does not assume equal variances, was used. When the assumption of normality was violated, appropriate nonparametric tests were applied, such as the Mann-Whitney *U* test for unpaired data or the Wilcoxon signed-rank test for paired data. For multiple *t* test, corrections for multiple comparisons were applied using the Holm-Sidak method. Reperfusion differences between the control and *Bmal1<sup>muscle</sup>* groups before and after surgery were compared using a generalized linear mixed-effects model, with the Geisser-Greenhouse correction applied to account for the reported death of 1 control mouse after surgery. Post hoc comparisons were performed using the Tukey test. Differences were considered statistically significant at  $P<0.05$ .

## RESULTS

### Disruption of Peripheral Circadian Clock in ECs and Skeletal Muscles of Patients With PAD

While earlier studies explored the roles of circadian clock in PAD pathogenesis using whole-body *Bmal1* knockout<sup>37</sup> and jet-leg<sup>38</sup> mouse models, a gap remains in distinguishing the contributions of the central clock from those in the peripheral tissue and cells. Interestingly, both studies found that the loss of core clock genes in ECs impairs functions such as proliferation, migration, and tube formation.<sup>37,38</sup> However, it is unknown whether the circadian clock is disrupted in ECs in patients with PAD. In our recent study,<sup>17</sup> we used the iPSC technology to generate ECs from patients with PAD (n=3) and age-matched healthy individuals (n=3; Figure 1A). Transcriptomic analysis revealed a significant reduction in the expression of genes associated with angiogenesis (Figure 1B), consistent with the endothelial dysfunction observed in patient iPSC-ECs. Furthermore, we identified a negative correlation in the expression of genes related to circadian rhythms when comparing iPSC-ECs derived from patients with PAD to those from healthy individuals, with a marked decrease in expression in iPSC-ECs derived from patients with PAD (Figure 1B). These included genes encoding core molecular clock regulators, such as *RORB*, *NFIL3*, *PER3*, *NR1D1*, *NR1D2*, and *NPAS2*, as well as genes known to be regulated by the circadian clock (Figure 1C).

Additionally, we analyzed the expression of molecular clock genes in skeletal muscles obtained from patients with PAD. Using an RNA-seq data set (GSE120642) from a prior study comparing muscle biopsies from healthy older adults and patients with CLI<sup>18</sup> (Figure 1D),

our gene set enrichment analysis indicated a negative correlation between CLI and genes involved in myogenesis (Figure 1E), which is consistent with previous reports of reduced calf muscle mass<sup>39</sup> in claudicating calf muscles.<sup>40</sup> Importantly, circadian-regulated genes including numerous core circadian regulators exhibited marked downregulation in the muscles of patients with CLI (Figure 1E; Figure S1), suggesting a potential link between circadian disruption and PAD skeletal muscle pathology. These findings collectively reveal disruptions in peripheral circadian clocks in both endothelial and skeletal muscle tissues in patients with PAD, shedding light on the potential implications for circadian timing in the peripheral tissues in the pathogenesis or severity of the disease.

### Loss of Skeletal Muscle *Bmal1* Impairs Perfusion Recovery in a Mouse Model of HLI

Given the severe muscle symptoms associated with PAD and our previous studies underscoring the essential role of the skeletal muscle circadian clock in hypoxia adaptation during exercise<sup>14</sup> and following myotoxin-induced injury,<sup>12</sup> we decided to investigate the yet unknown role of the muscle circadian clock in the progression and severity of PAD. To do this, we generated adult life-inducible skeletal muscle-specific *Bmal1* knockout mice (*Bmal1<sup>muscle</sup>*). This was achieved by crossbreeding *Bmal1<sup>lox</sup>* mice with *ACTA-rtTA-TRE-Cre* transgenic mice, as we have previously described.<sup>14</sup> *Bmal1* deletion in the skeletal muscle was triggered by administering concentrated doxycycline water via oral gavage for 3 consecutive days (Figure 2A). A week after the last oral gavage dose, both control (*Bmal1<sup>lox</sup>*; *ACTA-rtTA-TRE-Cre<sup>+/+</sup>*) and *Bmal1<sup>muscle</sup>* mice were confirmed their normal blood flow in both lower hind limbs via LDI (Figure S2) and subsequently underwent unilateral femoral artery ligation to simulate lower limb ischemia experienced in patients with PAD.<sup>41</sup> Perfusion in both hind limbs was monitored weekly via LDI, and the mice continued to consume doxycycline-infused water to ensure continued *Bmal1* deletion in both existing and newly regenerated myofibers. Reduction of the BMAL1 protein in gastrocnemius muscles from *Bmal1<sup>muscle</sup>* and control mice was confirmed by Western blotting analysis at the conclusion of the experiment (Figure 2B). Although there was a significant reduction in the absolute body weight change before and after the unilateral femoral ligation between *Bmal1<sup>muscle</sup>* and control mice (Figure S3A), the percentage of weight loss relative to the starting body weight in both groups was marginal ( $3.98\pm 2.33\%$  in control and  $3.52\pm 2.47\%$  in *Bmal1<sup>muscle</sup>* mice) and showed no significant difference between the 2 groups (Figure S3B), indicating similar doxycycline or surgery effects in mice of both groups. Notably, *Bmal1<sup>muscle</sup>* mice exhibited a marked delay in the recovery of limb perfusion following ischemic injury as

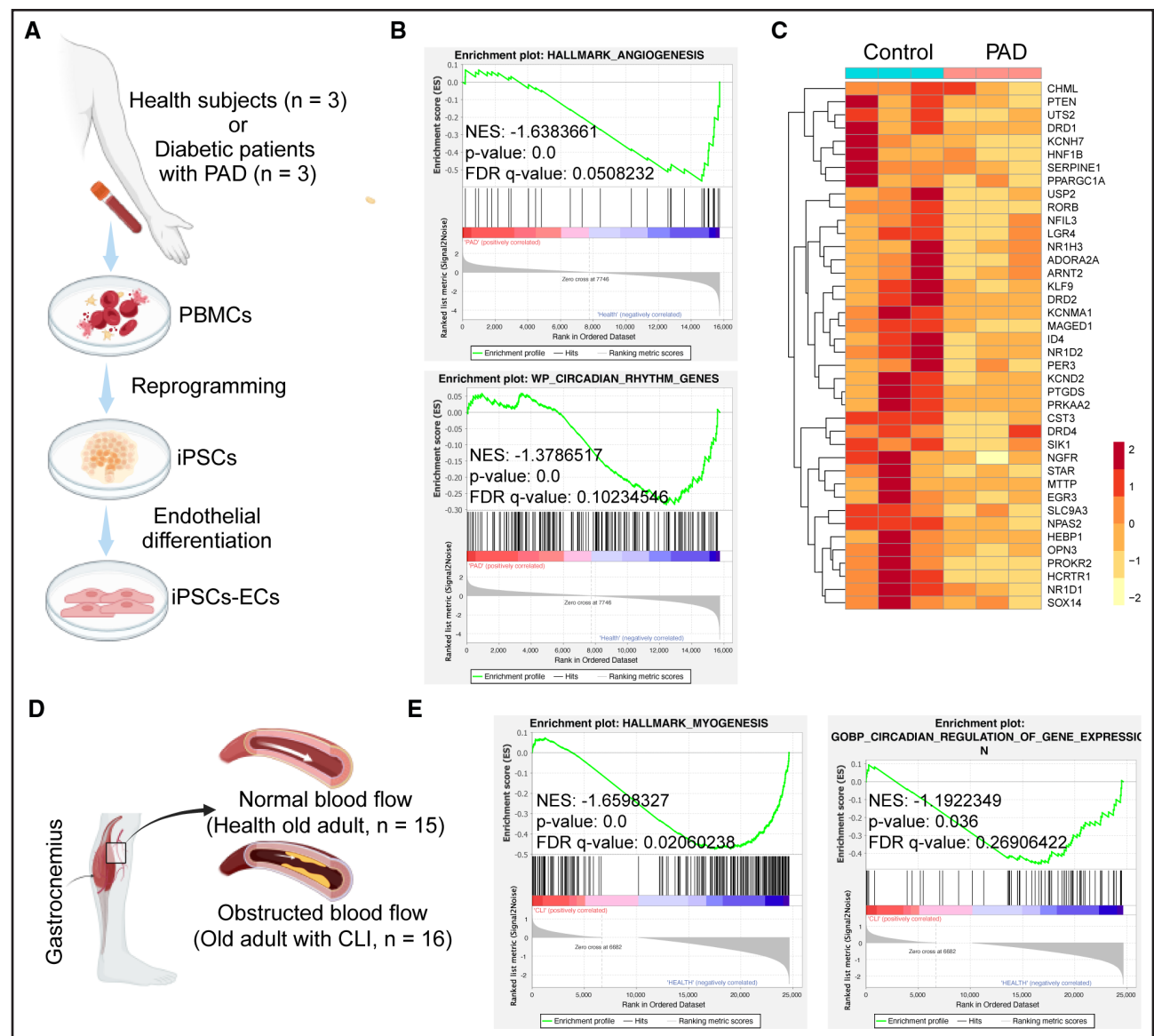


**Figure 1. Disrupted circadian clock gene expression in the endothelial cells (ECs) and skeletal muscle tissue of patients with peripheral artery disease (PAD).**

**A**, Schematic representation of the general process for generating induced pluripotent stem cell (iPSC)-derived ECs from blood samples of patients with PAD and age-matched healthy subjects using iPSC technology. Data derived from Gorashi et al.<sup>17</sup> **B**, Gene set enrichment analysis (GSEA) analysis of RNA-sequencing data set GSE236430, which includes iPSC-ECs from patients with PAD (n=3) and age-matched healthy subjects (n=3). **C**, Heatmap displaying the expression of genes associated with circadian rhythm in iPSC-ECs from patients with PAD compared with those from age-matched healthy subjects. The heatmap was generated using DESeq2-normalized counts. **D**, Schematic diagram showing the experimental design of the earlier study by Ryan et al.<sup>18</sup> performing transcriptome profiling on skeletal muscles from patients with PAD and healthy subjects. **E**, GSEA analysis of RNA-sequencing data set GSE120642, which includes gastrocnemius muscle samples from 16 patients with PAD and 15 age-matched healthy subjects. CLI indicates critical limb ischemia; FDR, false discovery rate; NES, normalized enrichment score; and PBMC, peripheral blood mononuclear cells.

compared with control mice (Figure 2C and 2D). These results highlight the crucial role of the skeletal muscle clock in managing limb ischemic reperfusion.

### Loss of Skeletal Muscle *Bmal1* Impairs Muscle Remodeling During Ischemia

Beyond limited limb perfusion, patients with PAD often face deteriorating muscle health with numerous limb

muscle pathologies such as weakness and exercise intolerance,<sup>42–44</sup> lower extremity muscular atrophy,<sup>2,42,45</sup> increased infiltrated fat tissue and intramuscular collagen deposition,<sup>46–48</sup> altered fiber type composition,<sup>43,44</sup> as well as reduced muscle oxidative capacity.<sup>2,49</sup> Therefore, we assessed the impact of muscle clock disruption on muscle remodeling under ischemia conditions. As anticipated, HLI triggered robust muscle remodeling, evidenced by the presence of numerous centrally nucleated

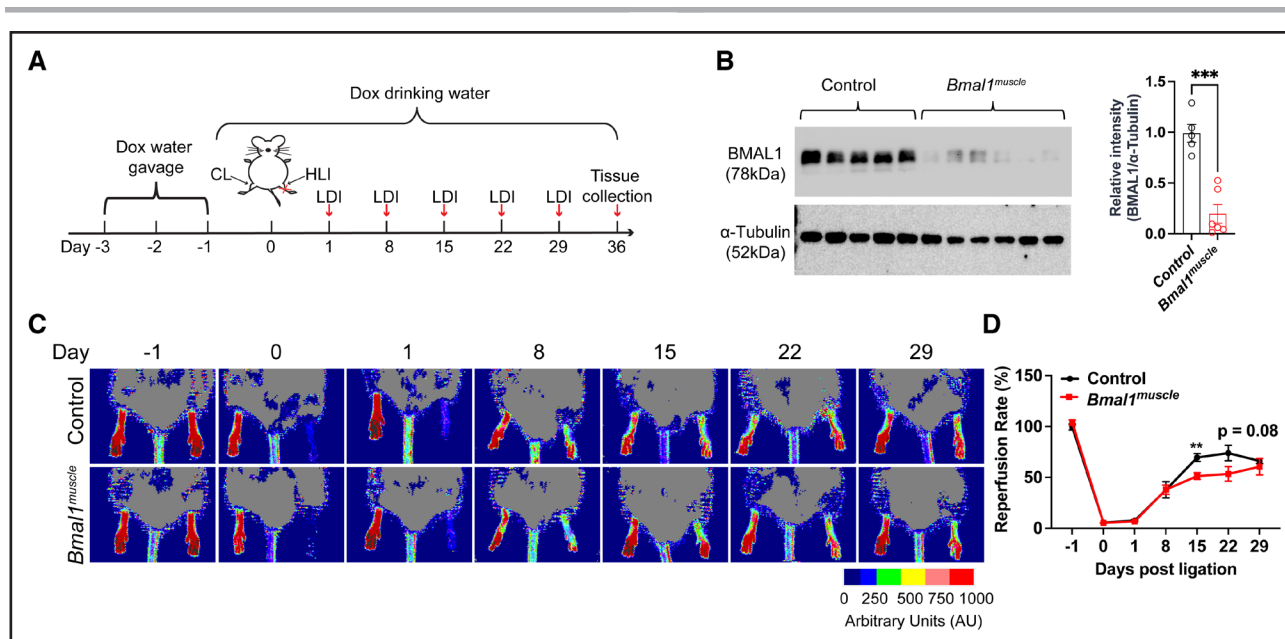


**Figure 2. Hindlimb ischemic (HLI) reperfusion in the HLI *Bmal1*<sup>muscle</sup> mice.**

**A**, Experimental design: *Bmal1*<sup>muscle</sup> (n=6) and control (n=5) mice received oral doxycycline (Dox) water for 3 days, followed by continuous Dox drinking water throughout the experimental duration. Unilateral femoral artery ligation surgery was performed on one side of the hind limb (HLI), while the contralateral (control limb [CL]) side remained uninjured. Limb perfusion was measured weekly using laser Doppler imaging (LDI). Tibialis anterior (TA) muscles from both sides of all experimental mice were collected on day 36 post-surgery. Color scale indicates perfusion units. **B**, Verification of BMAL1 (brain and muscle ARNT-like 1) expression with quantitative analysis by Western blotting in gastrocnemius muscles of *Bmal1*<sup>muscle</sup> (n=6) and control (n=5) mice. \*\*\**P*<0.001 by unpaired Student *t* test. **C**, LDI showing limb perfusion recovery in *Bmal1*<sup>muscle</sup> and control mice after induction of HLI. **D**, Quantification of limb perfusion over time (n=6 in the *Bmal1*<sup>muscle</sup> group and n=5 in the control group). Day -1 indicates the presurgery LDI value. \*\**P*<0.01, by a generalized linear mixed-effects model with the Geisser-Greenhouse correction.

myofibers in the TA muscles of the ischemic limb in both control and *Bmal1*<sup>muscle</sup> mice (Figure 3A). Despite the gastrocnemius muscle's proximity to the site of ligation, these muscles did not exhibit as severe and uniform levels of injury as observed in the TA muscles (Figure S4). Therefore, we focused on TA muscles in the subsequent studies. Notably, the TA muscles of the *Bmal1*<sup>muscle</sup> mice had a significant reduction in the number of regenerated myofibers compared with control mice (Figure 3B). Interestingly, it was observed that some nascent myofibers underwent hypertrophic growth in the absence of *Bmal1* (Figure 3A), as evidenced by their significantly increased average fiber size (Figure S5A) and rise in count of larger, newly formed myofibers (Figure 3C). Moreover, the proportion of type IIb myofibers, a dominant fast-twitch fiber type in mouse TA muscles,<sup>50</sup> exhibited a trended decrease in *Bmal1*<sup>muscle</sup> mice compared with controls (Figure 3D and 3E). Instead, the type IIA myofibers, another type of fast-twitch fiber, remained unchanged (Figure S5B and S5C). Importantly, the acute induction of *Bmal1* deletion did not prompt spontaneous muscle regeneration in the absence of injury (Figure S5D), and no significant differences were observed in the number and size of preexisting (noncentrally nucleated) myofibers between control and *Bmal1*<sup>muscle</sup> mice in the TA muscles of the nonoperated limbs (Figure S5E through S5G). In addition, we evaluated fat tissue infiltration in

the TA muscles of both sides in *Bmal1*<sup>muscle</sup> and control mice using oil red O staining. Although substantial fat tissue infiltration was observed in the TA muscles by day 36 post-surgery, no significant difference was observed between the 2 groups (Figure S6A and S6B). Similarly, no significant difference in fibrosis was observed in the TA muscles of either the ischemic limb or the contralateral limb, as indicated by Masson trichrome staining (Figure S6C and S6D). These findings imply that loss of circadian clock function in skeletal muscles leads to abnormal muscle regeneration and remodeling under ischemia conditions.

### Muscle Clock Disruption Alters the Expression of Genes Related to Metabolism and Muscle Development In Vivo

To explore the molecular mechanisms behind the observed angiogenic and myogenic phenotypes of the ischemic muscles of *Bmal1*<sup>muscle</sup> mice, we conducted transcriptomic analysis on TA muscles from both the ischemic (HLI) and contralateral (CL) limbs, harvested 36 days post-surgery from both control and *Bmal1*<sup>muscle</sup> mice (Figure 4A). RNA-seq revealed significant genotype- and treatment-dependent gene expression differences (Figure 4B). Specifically, 2322 and 1210 DEGs (adjusted *P*<0.05) were identified in the CL and HLI limbs of *Bmal1*<sup>muscle</sup> mice,

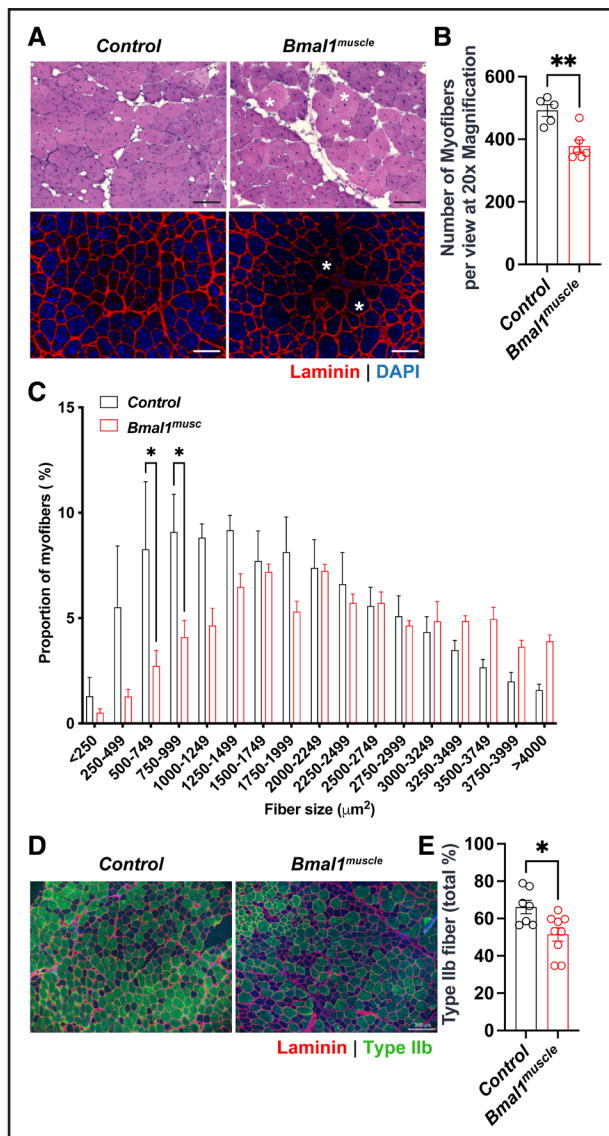


**Figure 3. Skeletal muscle remodeling in the *Bmal1*<sup>muscle</sup> hindlimb ischemia model.**

**A**, Representative hematoxylin and eosin and laminin/DAPI (4',6-diamidino-2-phenylindole) immunostaining on femoral artery (FA)-ligated tibialis anterior (TA) muscle cryosections from *Bmal1*<sup>muscle</sup> and control mice on day 36 post-surgery (scale bar=100  $\mu$ m). \*Hypertrophic myofibers. **B**, Comparison of the number of myofibers in the FA-ligated TA muscles between *Bmal1*<sup>muscle</sup> (n=6) and control (n=5) mice. \*\* $P < 0.01$  by Student *t* test. **C**, Nascent muscle fiber size (cross-sectional area) distribution in the FA-ligated TA muscles of *Bmal1*<sup>muscle</sup> (n=6) and control (n=5) mice. \* $P < 0.05$ , by multiple *t* test. **D**, Representative MYH4 (myosin heavy chain 4) immunohistochemistry for type IIb fiber type staining. Laminin immunostaining was applied to visualize borders of individual myofibers (scale bar=200  $\mu$ m). **E**, Quantification of the proportion of type IIb fibers in the FA-ligated TA muscles of *Bmal1*<sup>muscle</sup> (n=9) and control (n=7) mice. \* $P < 0.05$  by Student *t* test.

respectively, compared with controls (Figure 4C). By overlapping the DEGs in the CLs with previously identified rhythmically expressed genes (2330;  $P < 0.05$ ) in the gastrocnemius muscles of young adult (6-month-old) male mice,<sup>51</sup> we identified 524 genes that showed significant

changes in expression upon depletion of *Bmal1* (Figure S7A). Besides the genes involved in circadian rhythm regulation, many of the other oscillating genes were associated with hypoxia, TGF- $\beta$  (transforming growth factor- $\beta$ ), and myogenesis signaling pathways (Figure S7B). The KEGG pathway enrichment analysis showed that circadian rhythm-related genes were downregulated in the TA muscles of *Bmal1*<sup>muscle</sup> mice on both sides, validating the successful deletion of *Bmal1* in both existing and nascent myofibers (Figure 4D, left). Consistent with our previously uncovered role of the circadian clock in regulating hypoxic stress responses in the skeletal muscle via interactions with HIF1 $\alpha$ ,<sup>14</sup> we observed reduced expression of known HIF target genes, including the glycolytic enzymes *Hk2*, *Ldha*, *Slc2a3*, and *Vegfa*, a proangiogenic factor favoring EC proliferation and migration<sup>52</sup> (Table S1), in *Bmal1*<sup>muscle</sup>. Reduction in *Vegfa* expression was corroborated by quantitative PCR quantification (Figure 4E). We further measured extracellular VEGFA by ELISA and detected a significant reduction in the media derived from *Bmal1*-deficient myotubes compared with those from WT myotubes (Figure 4F). Additionally, mitochondrial respiration and oxidative phosphorylation-related genes were significantly upregulated in muscles lacking *Bmal1* (Figure 4D, right). Since our previous studies demonstrated that mitochondrial respiration is impaired in *Bmal1* null myotubes in hypoxia,<sup>14</sup> we predict that the upregulation of these genes indicates a compensatory effect for the impaired HIF1 $\alpha$ -mediated hypoxia adaptation. Another notable observation was the inactivation of TGF- $\beta$  signaling pathway in CL muscles of *Bmal1*<sup>muscle</sup> mice (Figure 4D, left). Among the genes linked to this signaling pathway, *Mstn*, a gene encoding a myokine that inhibits muscle growth,<sup>53</sup> was significantly downregulated, which was confirmed by quantitative PCR (Figure 4G). A notable decrease in intramuscular MSTN production was further verified in both the HLI and CLs on day 36 post-surgery via Western blot analysis (Figure 4H). Additionally, genes associated with tissue morphogenesis, differentiation, and development were downregulated in the CL muscles of *Bmal1*<sup>muscle</sup> mice, while genes related to ion transport (including calcium and potassium) and muscle contraction were upregulated genes in HLI muscles of *Bmal1*<sup>muscle</sup> mice compared with controls (Figure 4D, right). Overall, these data show widespread reprogramming of the clock-regulated transcriptome in the circadian clock-disrupted muscle tissue, both before and after exposure to ischemia, which may underlie the disrupted restoration of blood flow and myogenesis in FA-ligated limb muscles, consequently impeding normal muscle remodeling.

### Circadian Clock Disruption Alters the Expression of Genes Related to Metabolism and Myogenesis in Cultured Primary Myotubes

The RNA-seq data from skeletal muscle tissues on day 36 post-surgery offered insights into the transcriptome

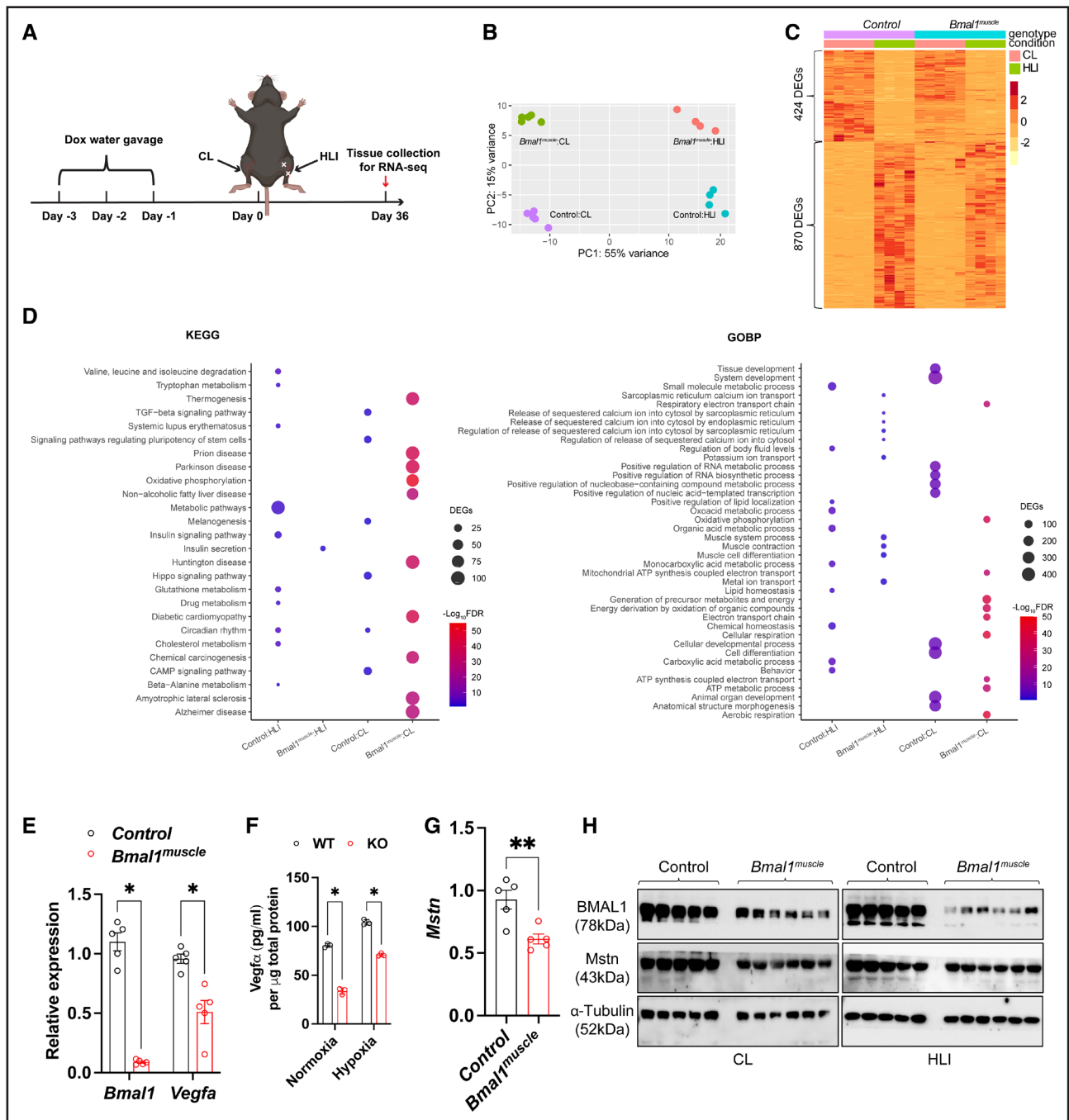


**Figure 4. Transcriptome profiling of tibialis anterior (TA) muscles in *Bmal1*<sup>muscle</sup> and control mice.**

**A**, Animal experimental design: induction of *Bmal1* knockout (KO) and hindlimb ischemia (HLI) surgery was conducted as described in Figure 2A. TA muscles with HLI and the contralateral control limb (CL) were collected on day 36 post-surgery for RNA-sequencing (RNA-seq) analysis. **B**, Principal component (PC) analysis of the transcriptome data. **C**, Heatmap showing differentially expressed genes (DEGs; adjusted  $P < 0.05$ ;  $-1 < \log_2$  fold change [FC]  $< 1$ ) in HLI and CL TA muscles between the *Bmal1*<sup>muscle</sup> (n=4) and control (n=4) groups. The heatmap was generated using DESeq2-normalized counts. **D**, The Kyoto Encyclopedia of Genes and Genomes (KEGG; left) and Gene Ontology Biological Processes (GOBP; right) signaling pathway enrichment analysis of the DEGs in HLI and CL TA muscles between the *Bmal1*<sup>muscle</sup> and control groups. **E**, Quantification of *Bmal1* and *Vegfa* mRNA levels in HLI TA muscles of *Bmal1*<sup>muscle</sup> (n=5) and control (n=5) mice by quantitative polymerase chain reaction (qPCR). \* $P < 0.05$  by Welch *t* test for *Bmal1* and standard *t* test for *Vegfa*. **F**, Measurement of VEGFA (vascular endothelial growth factor- $\alpha$ ) contents in media by ELISA. Primary myoblasts were isolated from male *Bmal1*<sup>lox/lox</sup> mice and induced in vitro into myotubes. The differentiated myotubes were infected with adenovirus expressing Cre recombinase or an empty vector (n=3 biological replicates per group) for 48 hours, followed by culturing under normoxia (21% O<sub>2</sub>) or hypoxia (1% O<sub>2</sub>) for 24 hours. \* $P < 0.05$  by 2-way ANOVA test. **G**, Quantification of *Mstn* (myostatin) mRNA levels in HLI TA muscles of *Bmal1*<sup>muscle</sup> (n=5) and control (n=5) mice by qPCR. \*\* $P < 0.01$  by Student *t* test. **H**, Verification of MSTN protein expression by Western blotting in HLI and CL TAs of *Bmal1*<sup>muscle</sup> (n=6) and control (n=5) mice. FDR indicates false discovery rate; and WT, wild type.

of largely recovered muscles but may not fully reveal the underlying mechanisms due to the lack of detailed transcriptional information and the variety of cell types in regenerating muscles after ischemic injury. To address these challenges, we utilized cultured myotubes to further investigate the antiangiogenic and antimyogenic phenotypes observed in *Bmal1<sup>muscle</sup>* mice with HLI. As depicted in Figure 5A, primary myoblasts were isolated from *Bmal1<sup>fx/fx</sup>* mice, expanded, and differentiated into myotubes (Figure S8A), with *Bmal1* deletion induced by Cre recombinase-expressing adenovirus. Control myotubes were infected with an empty adenovirus. These cells were then exposed to normal oxygen levels (21%) or 1% oxygen, simulating postsurgery intramuscular hypoxia. RNA-seq of these myotubes revealed genotype- and hypoxia-dependent DEGs (Figure 5B). Under normoxia, 1310 genes were upregulated and 1114 genes were downregulated in *Bmal1<sup>-/-</sup>* myotubes compared with wild type, while hypoxia exposure led to 1217 upregulated and 949 downregulated genes (Figure 5C). In normoxic myotubes, *Bmal1* deletion resulted in upregulation of genes related to mitochondrial respiration and ATP synthesis and downregulation of differentiation-associated genes (Figure 5D). Aerobic respiration genes were also upregulated in hypoxic *Bmal1<sup>-/-</sup>* myotubes (Figure 5D). There was a significant overlap in the upregulated and downregulated genes across different oxygen tensions (Figure S8B). Notably, hypoxia-responsive genes were commonly downregulated, whereas genes linked to oxidative phosphorylation and myogenesis were upregulated in *Bmal1<sup>-/-</sup>* myotubes (Figure S8C), indicating impaired hypoxia response and myogenesis in these cells.

### BMAL1 Regulates Transcriptional Activity or Expression of HIF, MyoD, and MEF2 Family Genes in Muscle Tissue In Vivo and in Cultured Myotubes

To identify transcription factor pathways that may participate in BMAL1-mediated actions during PAD, we performed DNA motif analysis on the promoter regions of genes significantly downregulated in *Bmal1*-deficient myotubes in hypoxia or ischemic TA muscles (following HLI) or in both conditions (common). As anticipated, DNA-binding motifs for HIF1 $\beta$ , a component of HIF complex,<sup>54</sup> and MyoD (myogenic differentiation 1), a key myogenic regulatory factor that directs muscle development<sup>55</sup> and maintenance of the fast IIB/IIX fiber type,<sup>56</sup> were enriched in the promoters of the genes that were downregulated in *Bmal1*-deleted muscles and myotubes as compared with controls (Figure 6A). Interestingly, the analysis also identified DNA-binding motifs for the MEF2 (myocyte enhancer factor 2) family members (eg, *Mef2a*, *Mef2c*, and *Mef2d*) in the promoters of those downregulated genes (Figure 6A). These results indicate a decrease in transcription activity of the MEF2 factors with *Bmal1* loss. Supporting this,

RNA-seq data showed significant reductions of *Myod*, *Mef2a*, *Mef2c*, and *Mef2d* expression in *Bmal1*-deficient TA muscles in the FA-ligated limb and myotubes under hypoxia compared with the corresponding controls (Figure 6B). Additionally, a previous study identified 2 regions homologous to MEF2-binding sites in the 5'-regulatory regions of the human *MSTN* gene,<sup>57</sup> suggesting that *Mef2* family members might directly bind to and regulate the *Mstn* expression. This was supported by the substantial reduction in *Mstn* expression following individual knock-downs of *Mef2* genes, including *Mef2a*, *Mef2c*, and *Mef2d* (Figure 6C). Additionally, we performed ATAC-seq on in vitro induced primary myotubes, using the same conditions as described for RNA-seq in Figure 5A. In general, we observed a decrease in the overall chromatin accessibility around transcriptional start site regions in *Bmal1<sup>-/-</sup>* myotubes compared with *Bmal1<sup>+/+</sup>* myotubes under both normoxic and hypoxic conditions (Figure 6D). Furthermore, integrating ATAC-seq and RNA-seq data revealed that genes downregulated at the mRNA levels, with concurrent reductions in chromatin accessibility near their transcriptional start site in *Bmal1<sup>-/-</sup>* versus *Bmal1<sup>+/+</sup>* myotubes, were predominantly associated with skeletal muscle tissue development and the regulation of skeletal muscle fiber development (Figure 6E). Notably, *Myod1* and *Mef2c*, 2 pivotal transcription factors in muscle development and myogenesis, were identified within the overlapping gene set, suggesting they may be directly regulated by circadian transcription factors. As previously reported, *Myod1* is a direct transcriptional target of the CLOCK/BMAL1 complex.<sup>58</sup> Indeed, ATAC-seq data from primary myoblast-derived myotubes showed a significant decrease in chromatin accessibility at the *Mef2c* promoter in the absence of *Bmal1* (Figure 6F), aligning with the reduced transcriptional activity observed in the RNA-seq data. We further analyzed a BMAL1 ChIP-sequencing data set (GSE143334) derived from pooled gastrocnemius muscle of C57BL/6J male mice, as reported in a previous study.<sup>59</sup> Our analysis revealed that BMAL1 binds to the transcription start site within the promoter of the *Mef2c* gene (Chromosome 7: 67 373 192–67 373 450; Figure 6F), indicating potentially direct transcriptional regulation of *Mef2c* by BMAL1. Collectively, these findings unveil a novel mechanism by which the circadian clock influences muscle regeneration under ischemic conditions.

## DISCUSSION

The murine HLI model is a widely used animal model to mimic the ischemic injuries experienced by patients with PAD.<sup>41</sup> While previous studies utilizing this model have predominantly focused on vascular aspects such as limb perfusion recovery and vascular density,<sup>60</sup> our current study goes beyond these parameters by characterizing skeletal muscle remodeling in response to HLI and uncovers significant insights into the molecular and

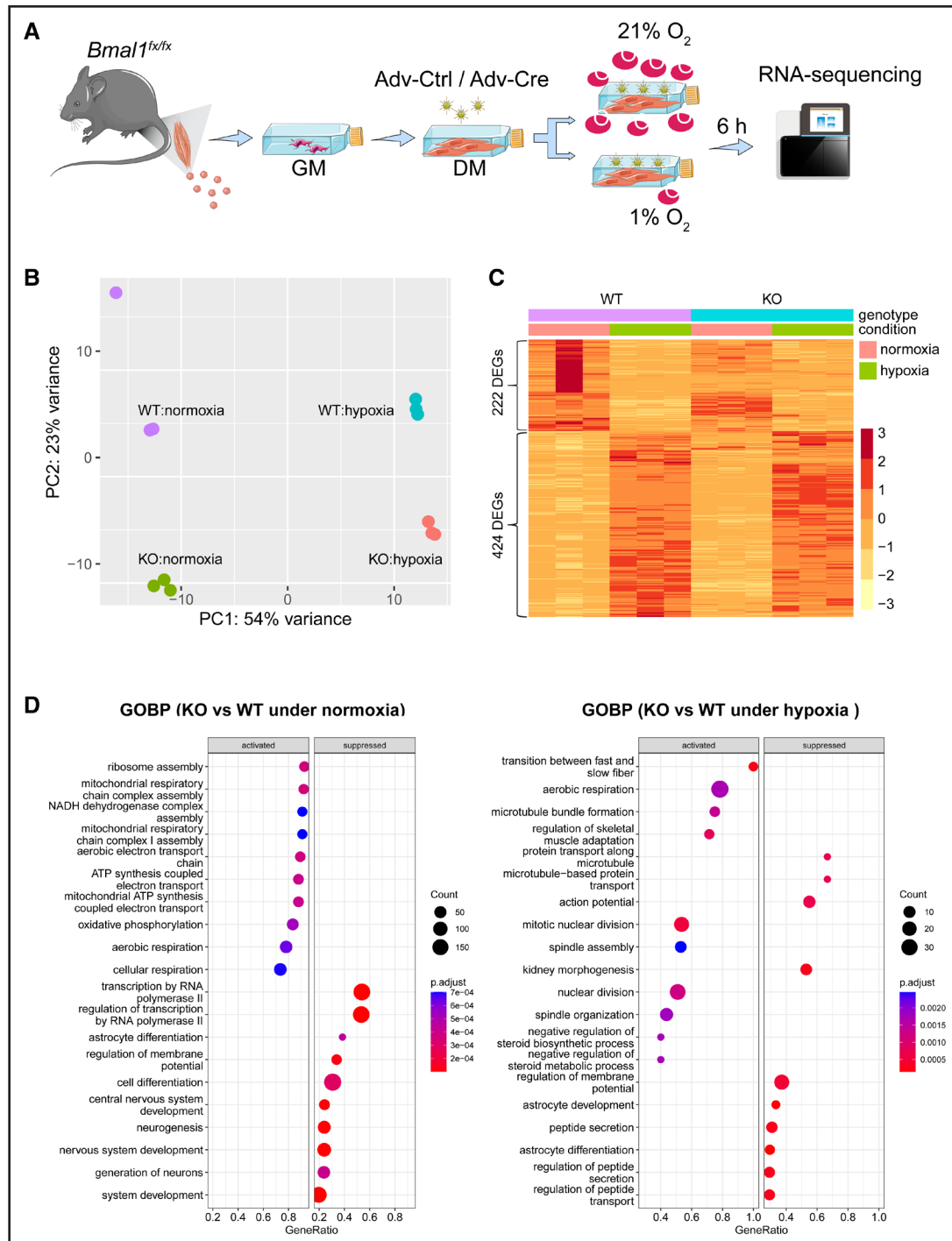


**Figure 5. Transcriptome profiling of *Bmal1* (brain and muscle ARNT-like 1)-deficient and control myotubes.**

**A**, Experimental design: primary myoblast isolation, differentiation, and adenovirus-induced *Bmal1* knockout in myotubes were conducted as described in Figure 4F. Adenovirus-infected myotubes were exposed to normoxia (21% O<sub>2</sub>) or hypoxia (1% O<sub>2</sub>) for 6 hours and then subjected to RNA-sequencing analysis (n=3 biological replicates per group). **B**, Principal component (PC) analysis of the transcriptome data. **C**, Heatmap showing differentially expressed genes (DEGs) in *Bmal1* knockout (KO) and wild-type (WT) myotubes under normoxia or hypoxia conditions. The heatmap was generated using DESeq2-normalized counts. **D**, Gene Ontology Biological Processes (GOBP) signaling pathway enrichment analysis of the DEGs in *Bmal1* KO and WT myotubes under normoxia or hypoxia conditions. GeneRatio represents the ratio of input genes that are annotated in a signaling pathway term. DM indicates differentiation medium; and GM, growth medium.

cellular changes occurring in the skeletal muscle following ischemia. Importantly, these results align with clinical observations of muscle pathology in patients with PAD. By expanding the focus beyond vascular outcomes to

include detailed analyses of muscle responses, our research provides a more holistic understanding of PAD and underscores the intricate interplay between circadian rhythms and tissue health. This novel perspective is

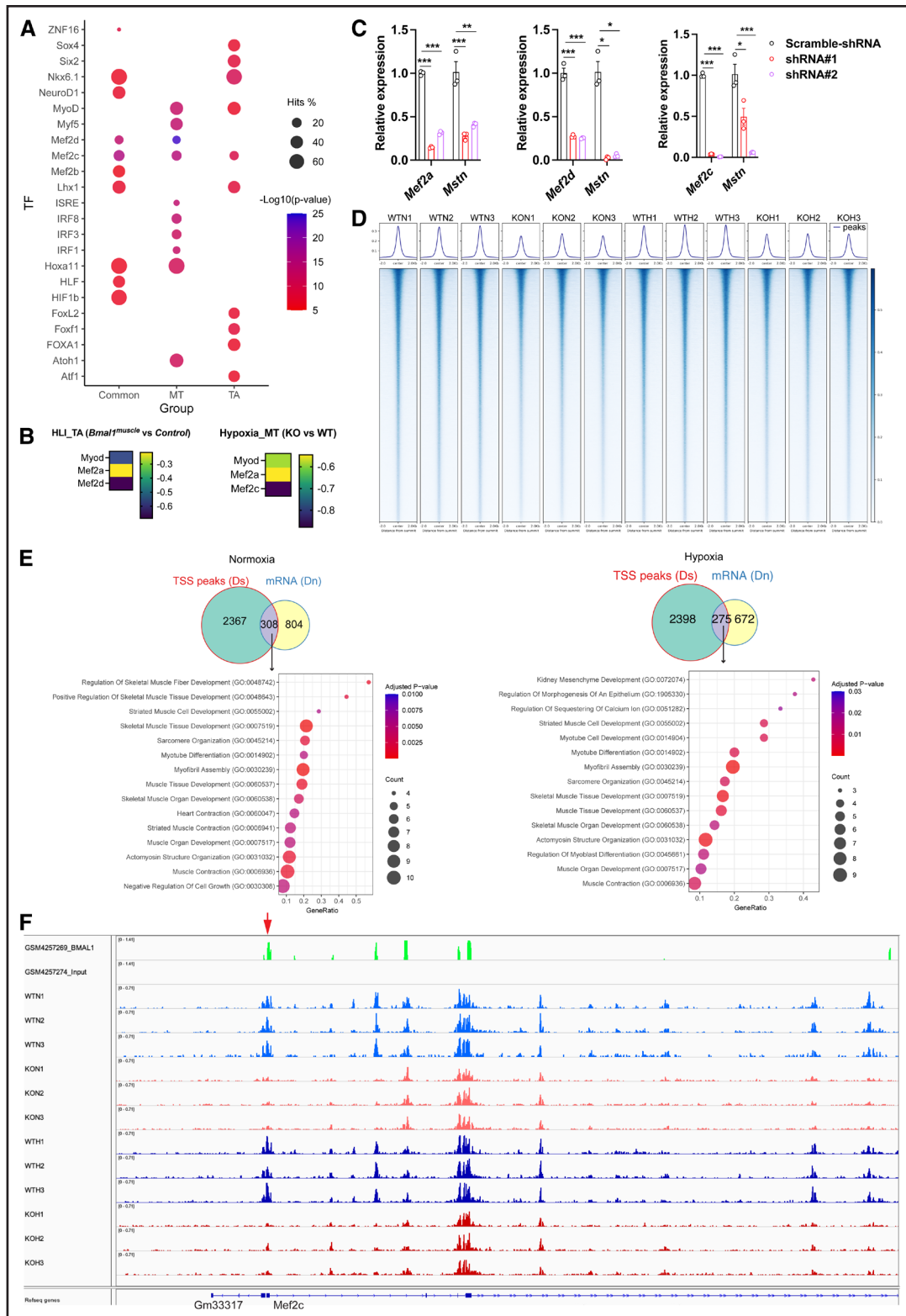


**Figure 6. Gene regulation of BMAL1 (brain and muscle ARNT-like 1) in tibialis anterior (TA) muscles and myotubes.**

**A**, DNA motif enrichment analysis within promoters of the significantly downregulated genes in hindlimb ischemia (HLI) TA muscles of *Bmal1*<sup>muscle</sup> vs control mice, *Bmal1*-deficient myotubes (MTs) vs wild-type (WT) myotubes under hypoxia, and the commonly downregulated genes between the TA muscles and myotubes. **B**, Heatmap illustrating the expression of *Myod*, *Mef2a*, and *Mef2c* in the HLI TA muscles of *Bmal1*<sup>muscle</sup> vs control mice or *Bmal1*-deficient myotubes vs WT myotubes under hypoxia. **C**, Quantification of *Mstn* mRNA expression in individual *Mef2* gene knockdown myotubes by quantitative polymerase chain reaction in biological triplicate. \* $P < 0.05$ , \*\* $P < 0.01$ , \*\*\* $P < 0.001$  by 1-way ANOVA comparing with the scramble-shRNA-infected group. **D**, Assay for transposase-accessible chromatin with sequencing (ATAC-seq) peak summit-centered heatmap (bottom) with an overlaid average profile (top) of ATAC-seq signal in control (WT) and (Continued)

crucial for developing comprehensive treatment strategies aimed at improving the quality of life for patients experiencing PAD.

Disrupting circadian rhythms can increase the risk of pathologies like cardiovascular disease, cancer, and metabolic syndrome. Mice with whole-body *Bmal1* knockout<sup>37</sup> or those subjected to jet lag<sup>38</sup> experience exacerbated PAD symptoms. Notably, among the various high-risk factors enumerated by the Centers for Disease Control and Prevention of the United States, blood pressure<sup>61</sup> and plasma cholesterol absorption/metabolism<sup>62</sup> follow the circadian rhythm, while smoking disrupts both central and peripheral circadian functions.<sup>63</sup> Other studies have shown mutual influences between circadian arrhythmia and atherosclerosis,<sup>64–66</sup> diabetes,<sup>67,68</sup> and aging.<sup>69,70</sup> While the molecular clock factors are active throughout the body, different tissue-specific clocks may have coordinated effects during PAD. ECs form the inner cellular lining of various blood vessels, including arteries, veins, and capillaries, as a monolayer of endothelium. Atherosclerosis is marked by phenotypic cell switching, in which ECs transition into mesenchymal stem cells.<sup>71</sup> The presence of endothelial-to-mesenchymal stem cell transition shows a strong correlation with the severity of atherosclerosis.<sup>72</sup> It has been demonstrated that endothelial-to-mesenchymal stem cell transition in cultured human umbilical vein ECs is accompanied by a substantial loss of CLOCK expression, while overexpression of CLOCK impedes this transition.<sup>73</sup> Additionally, BMAL1, the circadian binding partner of CLOCK, plays an anti-inflammatory role in human umbilical vein ECs by inhibiting lipid uptake.<sup>37</sup> Furthermore, another study reported that the circadian clock factor PER2 (Period 2) maintains cardiovascular function through the regulation of NO, vasodilatory prostaglandin production, and cyclooxygenase-1–derived vasoconstrictors.<sup>74</sup> Taken together, these studies raise the possibility that clocks in ECs may contribute to PAD pathology. However, the ultimate pathological consequence of PAD is loss of muscle mass, function, and ambulation. Thus, we feel it is crucial to understand the contribution of skeletal muscle-specific clocks to PAD and to understand their influences on muscle-intrinsic ischemia adaptation. In this study, we discovered that the expression of the circadian transcriptional activator BMAL1 in the skeletal muscle tissue during adult life is important for numerous aspects of muscle health, such as myofiber size and composition. Surprisingly, we also find that the muscle clock is important for ischemic limb reperfusion, suggesting muscle

clock-derived regulation of vascular repair. Together, these findings highlight the importance of muscle autonomous clocks in response to HLI injury.

CLI is marked by severe blockage of arteries in the lower limbs, leading to reduced blood flow and oxygen supply.<sup>75</sup> HIFs play a crucial role in mediating transcriptional reprogramming for hypoxia-adaptive responses.<sup>76</sup> Loss of HIF-1 $\alpha$  function hinders the expression of cytokines such as VEGF, stromal cell-derived factor 1, PDGF (platelet-derived growth factor), and angiotensin 1/2 and reduces the mobilization of angiogenic cells and the restoration of blood flow in the ischemic limbs of mice,<sup>16</sup> while overexpressing HIF-1 $\alpha$  enhances perfusion recovery following induction of HLI in older or diabetic mice.<sup>16</sup> These beneficial effects were attributed to both the mobilization of circulating angiogenic cells and the localized actions of angiogenic factors. Our previous studies demonstrate that clock disruption impairs HIF1 $\alpha$  stabilization and its transcriptional activity under hypoxic conditions,<sup>14</sup> thereby compromising skeletal muscle's response to acute exercise hypoxia<sup>14</sup> and muscle regeneration after injury induced by cardiotoxin.<sup>12</sup> This study reveals that skeletal muscles communicate with the endothelium through the active paracrine secretion of VEGFA, which is affected by the interaction between the circadian clock and HIF1 $\alpha$ -mediated hypoxic response signaling pathways. Notably, while clinical trials administering Neovascularin, a drug containing VEGFA,<sup>165</sup>-expressing plasmid, to patients with mild-to-severe claudication yielded a significant increase in pain-free walking distance in a 5-year follow-up study and 5-year postmarketing surveillance,<sup>77,78</sup> adverse effects such as the development of spider angioma and edema were observed in patients receiving VEGFA gene transfer.<sup>79</sup> Therefore, focusing on strengthening HIF transcriptional activity and simultaneously inducing a broad array of angiogenic factors via circadian rewiring presents a potentially superior therapeutic strategy for PAD.

An interesting observation in the ischemic limb of *Bmal1*<sup>muscle</sup> mice is the general reduction in the total fiber number accompanied by hypertrophic growth in certain, but not all, types of myofibers (Figure 3A through 3C). Patients with PAD often face muscle deterioration due to ischemia-induced atrophy<sup>80</sup> and increased levels of apoptosis.<sup>81</sup> Koutakis et al<sup>82</sup> reported in their study on biopsies taken from the gastrocnemius of 52 patients with PAD and 25 controls that both the relative frequency and size of type II fibers were lower, while those of type I and hybrid type I/II fibers were higher, in PAD

**Figure 6 Continued.** *Bmal1* knockout (KO) myotubes under normoxia (N) and hypoxia (H) conditions (n=3 biological replications per condition). The heatmap was generated based on normalized signal coverage calculated from bigWig files, centered on peak summits and extending 2 kb upstream and downstream. **E**, Gene ontology (GO) biological process analysis using genes exhibiting both downregulated mRNA expression in *Bmal1*<sup>-/-</sup> myotubes compared with WT, along with decreased chromatin accessibility near transcriptional start site (TSS) proximal regions under normoxia (**left**) and hypoxia (**right**) conditions. GeneRatio represents the ratio of input genes that are annotated in a signaling pathway term. **F**, Integrative Genomics Viewer genome browser tracks displaying BMAL1 binding from the publicly available chromatin immunoprecipitation-sequencing (ChIP-seq) data set (GSE143334) and our ATAC-seq reads from known promoter region (indicated by the red arrow) and the gene body of the *Mef2c* gene in the presence or absence of *Bmal1*. Dn indicates downregulation; and Ds, decrease.

compared with control gastrocnemius. This aligns with our observed decrease in the proportion of type IIb fibers in the nascent myofibers of *Bmal1<sup>muscle</sup>* mice compared with controls after femoral artery ligation (Figure 3D and 3E). We speculate that MSTN, a muscle growth inhibitory myokine,<sup>83,84</sup> may partially underlie this hypertrophic growth, given its significant downregulation in the muscles of *Bmal1<sup>muscle</sup>* mice compared with controls (Figure 4G and 4H). Notably, lack of MSTN, although promoting muscle hypertrophy, compromises force production and is associated with the loss of oxidative characteristics of the skeletal muscle.<sup>83</sup> Therefore, the appearance of those hypertrophic myofibers does not necessarily indicate increased strength but rather potential weakness. Indeed, both the specific force (muscle force per unit cross section)<sup>58</sup> and grip strength<sup>85</sup> are significantly lower in the muscles of adult life-induced skeletal muscle *Bmal1* knockout mice compared with controls.

An earlier study revealed that knockout of *Mstn* results in an increase in type IIb fibers while concomitantly decreasing type IIa and type I fibers.<sup>86</sup> This is due to the upregulation of *Mef2c*, an *MEF2* gene that plays important roles in type I fiber formation, and the downregulation of *Myod*, which is highly expressed in type II fibers.<sup>86</sup> In contrast, our results indicate that *MEF2* transcription factors are upstream regulators of *Mstn*, as knockdown of *Mef2* genes, including *Mef2a*, *Mef2c*, and *Mef2d*, leads to significant declines in *Mstn* expression (Figure 6C). This is consistent with a previous study identifying *MEF2*-binding sites in the 5' regulatory region of the murine<sup>87</sup> and human *MSTN* gene.<sup>57</sup> Instead, *BMAL1* potentially regulates *Mef2c* expression by directly binding to its promoter. Moreover, we observed decreases in *Myod* expression in both *Bmal1*-deficient TA muscles and myotubes (Figure 6B), potentially due to the rhythmic binding of *BMAL1/CLOCK* to the core enhancer of the *Myod* promoter,<sup>58</sup> which may account for the decrease in type IIb fibers in the absence of *Bmal1* (Figure 3D and 3E).

Taken together, our data suggest that *BMAL1* coordinates the HIF1 $\alpha$ -mediated hypoxia response, affecting *Vegfa* expression, which hinders angiogenesis and underlies the defect in muscle reperfusion following induction of HLI. In addition, *BMAL1* also regulates *Mstn* expression via *Mef2* family transcription factors. The reduction in *MSTN* production in *Bmal1*-deficient muscles may lead to muscle hypertrophy during ischemic muscle regeneration, contributing to muscle weakness in PAD. Finally, clock-controlled *Myod* expression may be crucial in maintaining skeletal muscle fiber type under limb ischemia conditions. Targeting muscle circadian arrhythmia is a potential therapeutic approach mitigating perfusion deficits and pathogenic muscle conditions in patients with PAD.

While our study provides significant insights into the role of the circadian transcriptional activator *BMAL1* in

skeletal muscle health and ischemic responses in an HLI mouse model, there are several limitations that should be considered. First, we did not include female mice in our study. This is a critical limitation as sex differences can significantly influence the outcomes in cardiovascular and muscle-related pathologies. Future studies should include both male and female mice to better understand the potential sex-specific effects of *BMAL1* in PAD and related conditions. Second, the decline in type IIb fibers observed in the absence of *BMAL1* in our mouse model needs to be further investigated in the context of human patients with PAD. Human skeletal muscles do not contain type IIb fibers, which are present in rodents. This difference limits the direct applicability of our findings to human physiology. Additional research and sample size are needed to explore how *BMAL1* influences other fiber types in human muscles and to establish a more accurate model for studying human PAD and enhance the translational potential of these findings.

## Translational Outlook

Our study raises several potential clinical implications for vascular disease as our findings further support the role of circadian dysfunction in the role of cardiovascular disease pathogenesis. Circadian-based interventions thus hold promise in potentially blunting the progression and severity of PAD. Chronotherapies are an intuitive first option, in which drug therapies consider both circadian pharmacokinetics and pharmacodynamics alongside disease physiology. For instance, timing of antihypertensive administration produces varying effects on 24-hour blood pressure with potential downstream effects on cardiovascular remodeling.<sup>88</sup> Similarly, timing of antiplatelet administration produces significant variation in maximal effect, which can be tuned to match periods of maximal platelet reactivity.<sup>89</sup> Acute limb ischemic events share a morning peak and nocturnal nadir, akin to other thrombotic events, such as myocardial infarction.<sup>90</sup> Thus, strategies to treat PAD may benefit from chronotherapeutic delivery to optimize therapeutic efficacy. Late manifestations of PAD, including gangrene, may also exhibit circadian variation and may similarly benefit from chronotherapies.<sup>91</sup> The exact mechanistic underpinnings of these events remain an ongoing area of research with significant translational potential.

Alternatively, restoration of the clock itself is another promising strategy. Pharmaceutical chronobiotics can aid with clock entrainment in settings of circadian dysfunction. Well-established therapies include melatonin, which has demonstrated efficacy in reducing fat mass or glycosylated hemoglobin in nonvascular patients.<sup>92,93</sup> Similar trials have not been conducted in the PAD population, and, while promising, the applicability of these findings should remain tempered. Nonpharmacological clock restoration includes behavioral modifications such as modulation of light exposure or exercise therapy.<sup>94,95</sup>

Specifically, supervised exercise therapy when paired with revascularization may provide the largest improvement in walking distance and quality of life in claudicants and is furthermore covered by Medicare and Medicaid.<sup>96,97</sup> And while the positive impact of exercise therapy is likely multifactorial, there likely exists some benefit conferred via clock restoration.

Last, tissue-specific clock function as an anticipatory sensor of the external environment particularly highlights the potential for local circadian-based therapies.<sup>64</sup> Calf musculature is simultaneously the most prone to ischemia secondary to PAD while also under significant metabolic demand during ambulation, as evidenced by the symptoms of intermittent claudication or chronic limb-threatening ischemia. Delivery of intramuscular cellular therapies as a strategy to combat chronic limb-threatening ischemia in patients unsuitable for revascularization has already reached clinical translation with modest effects.<sup>98</sup> Restoration of muscle-specific circadian rhythm is thus an intuitive therapeutic target as functional metrics, such as walking distance, are dependent on muscle health in general and not perfusion alone. Major challenges include determining an optimal interventional range as integrated circadian feedback regulation may result in unexpected results of clock manipulation.<sup>99</sup> Similarly, the use of nocturnal animals as a testbed for circadian therapies remains a limitation in translating therapies to a diurnal species (human).<sup>99</sup> Strategies to locally deliver therapies such as NAD<sup>+</sup> (nicotinamide adenine dinucleotide) are an ongoing area of intense research by our group and others. Collaboration between circadian biologists, biomedical engineers, and clinicians will remain paramount in designing a translatable therapy that accounts for the intricate circadian network, optimized release kinetics, and the clinical workflow.

## ARTICLE INFORMATION

Received August 28, 2024; accepted November 18, 2024.

### Affiliations

Department of Biochemistry and Molecular Genetics (P.Z., A.W.T.S., N.X.H., E.M.P., C.B.P.), Department of Medicine, Division of Endocrinology, Metabolism and Molecular Medicine (P.Z., A.W.T.S., N.X.H., E.M.P., C.B.P.), and Department of Surgery, Division of Vascular Surgery (C.L.C., C.D., B.J.), Northwestern University Feinberg School of Medicine, Chicago, IL. Department of Biomedical Engineering, McCormick School of Engineering, Northwestern University, Chicago, IL (B.J.).

### Sources of Funding

This research was supported by the National Institutes of Health (NIH) National Institute of Diabetes and Digestive and Kidney Diseases grants R01DK123358 and P30DK020595 (C.B. Peek) and NIH National Heart, Lung, and Blood Institute grant 5T32HL094293-14 (C.L. Chao).

### Disclosures

None.

### Supplemental Material

Tables S1 and S2  
 Figures S1–S8  
 Major Resources Table  
 Raw Unedited Immunoblot Images

## REFERENCES

- Criqui MH, Matsushita K, Aboyans V, Hess CN, Hicks CW, Kwan TW, McDermott MM, Misra S, Ujmeta F; American Heart Association Council on Epidemiology and Prevention; Council on Arteriosclerosis, Thrombosis and Vascular Biology; Council on Cardiovascular Radiology and Intervention; Council on Lifestyle and Cardiometabolic Health; Council on Peripheral Vascular Disease; and Stroke Council. Lower extremity peripheral artery disease: contemporary epidemiology, management gaps, and future directions: a scientific statement from the American Heart Association. *Circulation*. 2021;144:e171–e191. doi: 10.1161/CIR.0000000000001005
- McDermott MM, Ferrucci L, Gonzalez-Freire M, Kosmac K, Leeuwenburgh C, Peterson CA, Saini S, Sufit R. Skeletal muscle pathology in peripheral artery disease: a brief review. *Arterioscler Thromb Vasc Biol*. 2020;40:2577–2585. doi: 10.1161/ATVBAHA.120.313831
- Bass J, Lazar MA. Circadian time signatures of fitness and disease. *Science*. 2016;354:994–999. doi: 10.1126/science.aah4965
- Li X, Liu X, Meng Q, Wu X, Bing X, Guo N, Zhao X, Hou X, Wang B, Xia M, et al. Circadian clock disruptions link oxidative stress and systemic inflammation to metabolic syndrome in obstructive sleep apnea patients. *Front Physiol*. 2022;13:932596. doi: 10.3389/fphys.2022.932596
- Abdelsattar ZM, Hendren S, Wong SL, Campbell DA Jr, Ramachandran SK. The impact of untreated obstructive sleep apnea on cardiopulmonary complications in general and vascular surgery: a cohort study. *Sleep*. 2015;38:1205–1210. doi: 10.5665/sleep.4892
- Peek CB, Ramsey KM, MarcheVA B, Bass J. Nutrient sensing and the circadian clock. *Trends Endocrinol Metab*. 2012;23:312–318. doi: 10.1016/j.tem.2012.02.003
- Takahashi JS. Molecular components of the circadian clock in mammals. *Diabetes Obes Metab*. 2015;17:6–11. doi: 10.1111/dom.12514
- Harfmann BD, Schroder EA, Esser KA. Circadian rhythms, the molecular clock, and skeletal muscle. *J Biol Rhythms*. 2015;30:84–94. doi: 10.1177/0748730414561638
- Schiaffino S, Blaauw B, Dyar KA. The functional significance of the skeletal muscle clock: lessons from Bmal1 knockout models. *Skelet Muscle*. 2016;6:33. doi: 10.1186/s13395-016-0107-5
- Paschos GK, FitzGerald GA. Circadian clocks and vascular function. *Circ Res*. 2010;106:833–841. doi: 10.1161/CIRCRESAHA.109.211706
- Astone M, Oberkersch RE, Tosi G, Biscotini A, Santoro MM. The circadian protein BMAL1 supports endothelial cell cycle during angiogenesis. *Cardiovasc Res*. 2023;119:1952–1968. doi: 10.1093/cvr/cvad057
- Zhu P, Hamlish NX, Thakkar AV, Steffek AWT, Rendleman EJ, Khan NH, Waldeck NJ, DeVilbiss AW, Martin-Sandoval MS, Mathews TP, et al. BMAL1 drives muscle repair through control of hypoxic NAD(+) regeneration in satellite cells. *Genes Dev*. 2022;36:149–166. doi: 10.1101/gad.349066.121
- Zhu P, Peek CB. Circadian timing of satellite cell function and muscle regeneration. *Curr Top Dev Biol*. 2024;158:307–339. doi: 10.1016/bs.ctdb.2024.01.017
- Peek CB, Levine DC, Cedernaes J, Taguchi A, Kobayashi Y, Tsai SJ, Bonar NA, McNulty MR, Ramsey KM, Bass J. Circadian clock interaction with HIF1alpha mediates oxygenic metabolism and anaerobic glycolysis in skeletal muscle. *Cell Metab*. 2017;25:86–92. doi: 10.1016/j.cmet.2016.09.010
- Ho TK, Abraham DJ, Black CM, Baker DM. Hypoxia-inducible factor 1 in lower limb ischemia. *Vascular*. 2006;14:321–327. doi: 10.2310/6670.2006.00056
- Bosch-Marce M, Okuyama H, Wesley JB, Sarkar K, Kimura H, Liu YV, Zhang H, Strazza M, Rey S, Savino L, et al. Effects of aging and hypoxia-inducible factor-1 activity on angiogenic cell mobilization and recovery of perfusion after limb ischemia. *Circ Res*. 2007;101:1310–1318. doi: 10.1161/CIRCRESAHA.107.153346
- Gorashi R, Rivera-Bolanos N, Dang C, Chai C, Kovacs B, Alharbi S, Ahmed SS, Goyal Y, Ameer G, Jiang B. Modeling diabetic endothelial dysfunction with patient-specific induced pluripotent stem cells. *Bioeng Transl Med*. 2023;8:e10592. doi: 10.1002/btm.2.10592
- Ryan TE, Yamaguchi DJ, Schmidt CA, Zeczycki TN, Shaikh SR, Brophy P, Green TD, Tarpey MD, Karnekar R, Goldberg EJ, et al. Extensive skeletal muscle cell mitochondriopathy distinguishes critical limb ischemia patients from claudicants. *JCI Insight*. 2018;3:e123235. doi: 10.1172/jci.insight.123235
- Mootha VK, Lindgren CM, Eriksson KF, Subramanian A, Sihag S, Lehar J, Puigserver P, Carlsson E, Ridderstrale M, Laurila E, et al. PGC-1alpha-responsive genes involved in oxidative phosphorylation are coordinately downregulated in human diabetes. *Nat Genet*. 2003;34:267–273. doi: 10.1038/ng1180
- Subramanian A, Tamayo P, Mootha VK, Mukherjee S, Ebert BL, Gillette MA, Paulovich A, Pomeroy SL, Golub TR, Lander ES, et al. Gene set enrichment

- analysis: a knowledge-based approach for interpreting genome-wide expression profiles. *Proc Natl Acad Sci USA*. 2005;102:15545–15550. doi: 10.1073/pnas.0506580102
21. Tamayo P, Steinhardt G, Liberzon A, Mesirov JP. The limitations of simple gene set enrichment analysis assuming gene independence. *Stat Methods Med Res*. 2016;25:472–487. doi: 10.1177/0962280212460441
  22. Johnson BP, Walisser JA, Liu Y, Shen AL, McDearmon EL, Moran SM, McIntosh BE, Vollrath AL, Schook AC, Takahashi JS, et al. Hepatocyte circadian clock controls acetaminophen bioactivation through NADPH-cytochrome P450 oxidoreductase. *Proc Natl Acad Sci USA*. 2014;111:18757–18762. doi: 10.1073/pnas.1421708111
  23. Rahmati M, Rashno A. Automated image segmentation method to analyse skeletal muscle cross section in exercise-induced regenerating myofibers. *Sci Rep*. 2021;11:21327. doi: 10.1038/s41598-021-00886-3
  24. Ruifrok AC, Johnston DA. Quantification of histochemical staining by color deconvolution. *Anal Quant Cytol Histol*. 2001;23:291–299.
  25. Bolger AM, Lohse M, Usadel B. Trimmomatic: a flexible trimmer for Illumina sequence data. *Bioinformatics*. 2014;30:2114–2120. doi: 10.1093/bioinformatics/btu170
  26. Dobin A, Davis CA, Schlesinger F, Drenkow J, Zaleski C, Jha S, Batut P, Chaisson M, Gingeras TR. STAR: ultrafast universal RNA-seq aligner. *Bioinformatics*. 2013;29:15–21. doi: 10.1093/bioinformatics/bts635
  27. Li B, Dewey CN. RSEM: accurate transcript quantification from RNA-Seq data with or without a reference genome. *BMC Bioinf*. 2011;12:323. doi: 10.1186/1471-2105-12-323
  28. Love MI, Huber W, Anders S. Moderated estimation of fold change and dispersion for RNA-seq data with DESeq2. *Genome Biol*. 2014;15:550. doi: 10.1186/s13059-014-0550-8
  29. Sonesson C, Love MI, Robinson MD. Differential analyses for RNA-seq: transcript-level estimates improve gene-level inferences. *F1000Res*. 2015;4:1521. doi: 10.12688/f1000research.7563.2
  30. Kuleshov MV, Jones MR, Rouillard AD, Fernandez NF, Duan Q, Wang Z, Koplev S, Jenkins SL, Jagodnik KM, Lachmann A, et al. Enrichr: a comprehensive gene set enrichment analysis web server 2016 update. *Nucleic Acids Res*. 2016;44:W90–W97. doi: 10.1093/nar/gkw377
  31. Yu G, Wang LG, Han Y, He QY. clusterProfiler: an R package for comparing biological themes among gene clusters. *OMICS*. 2012;16:284–287. doi: 10.1089/omi.2011.0118
  32. Heinz S, Benner C, Spann N, Bertolino E, Lin YC, Laslo P, Cheng JX, Murre C, Singh H, Glass CK. Simple combinations of lineage-determining transcription factors prime cis-regulatory elements required for macrophage and B cell identities. *Mol Cell*. 2010;38:576–589. doi: 10.1016/j.molcel.2010.05.004
  33. Langmead B, Salzberg SL. Fast gapped-read alignment with Bowtie 2. *Nat Methods*. 2012;9:357–359. doi: 10.1038/nmeth.1923
  34. Reske JJ, Wilson MR, Chandler RL. ATAC-seq normalization method can significantly affect differential accessibility analysis and interpretation. *Epi-genetics Chromatin*. 2020;13:22. doi: 10.1186/s13072-020-00342-y
  35. Ramirez F, Ryan DP, Gruning B, Bhardwaj V, Kilpert F, Richter AS, Heyne S, Dundar F, Manke T. deepTools2: a next generation web server for deep-sequencing data analysis. *Nucleic Acids Res*. 2016;44:W160–W165. doi: 10.1093/nar/gkw257
  36. Sarbassov DD, Guertin DA, Ali SM, Sabatini DM. Phosphorylation and regulation of Akt/PKB by the rictor-mTOR complex. *Science*. 2005;307:1098–1101. doi: 10.1126/science.1106148
  37. Xu L, Liu Y, Cheng Q, Shen Y, Yuan Y, Jiang X, Li X, Guo D, Jiang J, Lin C. Bmal1 downregulation worsens critical limb ischemia by promoting inflammation and impairing angiogenesis. *Front Cardiovasc Med*. 2021;8:712903. doi: 10.3389/fcvm.2021.712903
  38. Tsuzuki K, Shimizu Y, Suzuki J, Pu Z, Yamaguchi S, Fujikawa Y, Kato K, Ohashi K, Takefuji M, Bando YK, et al. Adverse effect of circadian rhythm disorder on reparative angiogenesis in hind limb ischemia. *J Am Heart Assoc*. 2021;10:e020896. doi: 10.1161/JAHA.121.020896
  39. McDermott MM, Hoff F, Ferrucci L, Pearce WH, Guralnik JM, Tian L, Liu K, Schneider JR, Sharma L, Tan J, et al. Lower extremity ischemia, calf skeletal muscle characteristics, and functional impairment in peripheral arterial disease. *J Am Geriatr Soc*. 2007;55:400–406. doi: 10.1111/j.1532-5415.2007.01092.x
  40. Pipinos II, Shepard AD, Anagnostopoulos PV, Katsamouris A, Boska MD. Phosphorus 31 nuclear magnetic resonance spectroscopy suggests a mitochondrial defect in claudicating skeletal muscle. *J Vasc Surg*. 2000;31:944–952. doi: 10.1067/mva.2000.106421
  41. Niiyama H, Huang NF, Rollins MD, Cooke JP. Murine model of hindlimb ischemia. *J Vis Exp*. 2009;23:1035. doi: 10.3791/1035
  42. Koutakis P, Myers SA, Cluff K, Ha DM, Haynatzki G, McComb RD, Uchida K, Miserlis D, Papoutsis E, Johanning JM, et al. Abnormal myofiber morphology and limb dysfunction in claudication. *J Surg Res*. 2015;196:172–179. doi: 10.1016/j.jss.2015.02.011
  43. Regensteiner JG, Wolfel EE, Brass EP, Carry MR, Ringel SP, Hargarten ME, Stamm ER, Hiatt WR. Chronic changes in skeletal muscle histology and function in peripheral arterial disease. *Circulation*. 1993;87:413–421. doi: 10.1161/01.cir.87.2.413
  44. Askew CD, Green S, Walker PJ, Kerr GK, Green AA, Williams AD, Febbraio MA. Skeletal muscle phenotype is associated with exercise tolerance in patients with peripheral arterial disease. *J Vasc Surg*. 2005;41:802–807. doi: 10.1016/j.jvs.2005.01.037
  45. Makitie J, Teravainen H. Histochemical changes in striated muscle in patients with intermittent claudication. *Arch Pathol Lab Med*. 1977;101:658–663.
  46. Miettinen CJ, Lackner TJ, Karvelis PS, Willcockson GT, Shields CM, Lambert NG, Koutakis P, Fuglestad MA, Hernandez H, Haynatzki GR, et al. Abnormal microvascular architecture, fibrosis, and pericyte characteristics in the calf muscle of peripheral artery disease patients with claudication and critical limb ischemia. *J Clin Med*. 2020;9:2575. doi: 10.3390/jcm9082575
  47. Ismaeel A, Miserlis D, Papoutsis E, Haynatzki G, Bohannon WT, Smith RS, Eidson JL, Casale GP, Pipinos II, Koutakis P. Endothelial cell-derived pro-fibrotic factors increase TGF-beta1 expression by smooth muscle cells in response to cycles of hypoxia-hyperoxia. *Biochim Biophys Acta Mol Basis Dis*. 2022;1868:166278. doi: 10.1016/j.bbdis.2021.166278
  48. Ding N, Yang C, Ballew SH, Kalbaugh CA, McEvoy JW, Salameh M, Aguilar D, Hoogeveen RC, Nambi V, Selvin E, et al. Fibrosis and inflammatory markers and long-term risk of peripheral artery disease: the ARIC study. *Arterioscler Thromb Vasc Biol*. 2020;40:2322–2331. doi: 10.1161/ATVBAHA.120.314824
  49. White SH, McDermott MM, Sufit RL, Kosmac K, Bugg AW, Gonzalez-Freire M, Ferrucci L, Tian L, Zhao L, Gao Y, et al. Walking performance is positively correlated to calf muscle fiber size in peripheral artery disease subjects, but fibers show aberrant mitophagy: an observational study. *J Transl Med*. 2016;14:284. doi: 10.1186/s12967-016-1030-6
  50. Giacomello E, Crea E, Torelli L, Bergamo A, Reggiani C, Sava G, Toniolo L. Age dependent modification of the metabolic profile of the tibialis anterior muscle fibers in C57BL/6J mice. *Int J Mol Sci*. 2020;21:3923. doi: 10.3390/ijms21113923
  51. Wolff CA, Gutierrez-Monreal MA, Meng L, Zhang X, Douma LG, Costello HM, Douglas CM, Ebrahimi E, Pham A, Oliveira AC, et al. Defining the age-dependent and tissue-specific circadian transcriptome in male mice. *Cell Rep*. 2023;42:111982. doi: 10.1016/j.celrep.2022.111982
  52. Shibuya M. Vascular endothelial growth factor (VEGF) and its receptor (VEGFR) signaling in angiogenesis: a crucial target for anti- and pro-angiogenic therapies. *Genes Cancer*. 2011;2:1097–1105. doi: 10.1177/1947601911423031
  53. Chen MM, Zhao YP, Zhao Y, Deng SL, Yu K. Regulation of myostatin on the growth and development of skeletal muscle. *Front Cell Dev Biol*. 2021;9:785712. doi: 10.3389/fcell.2021.785712
  54. Semenza GL. Hypoxia-inducible factors in physiology and medicine. *Cell*. 2012;148:399–408. doi: 10.1016/j.cell.2012.01.021
  55. Hernandez-Hernandez JM, Garcia-Gonzalez EG, Brun CE, Rudnicki MA. The myogenic regulatory factors, determinants of muscle development, cell identity and regeneration. *Semin Cell Dev Biol*. 2017;72:10–18. doi: 10.1016/j.semcdb.2017.11.010
  56. Hughes SM, Koishi K, Rudnicki M, Maggs AM. MyoD protein is differentially accumulated in fast and slow skeletal muscle fibres and required for normal fibre type balance in rodents. *Mech Dev*. 1997;61:151–163. doi: 10.1016/s0925-4773(96)00631-4
  57. Ma K, Mallidis C, Artaza J, Taylor W, Gonzalez-Cadavid N, Bhasin S. Characterization of 5'-regulatory region of human myostatin gene: regulation by dexamethasone in vitro. *Am J Physiol Endocrinol Metab*. 2001;281:E1128–E1136. doi: 10.1152/ajpendo.2001.281.6.E1128
  58. Andrews JL, Zhang X, McCarthy JJ, McDearmon EL, Hornberger TA, Russell B, Campbell KS, Arbogast S, Reid MB, Walker JR, et al. CLOCK and BMAL1 regulate MyoD and are necessary for maintenance of skeletal muscle phenotype and function. *Proc Natl Acad Sci USA*. 2010;107:19090–19095. doi: 10.1073/pnas.1014523107
  59. Gabriel BM, Altintas A, Smith JAB, Sardon-Puig L, Zhang X, Basse AL, Laker RC, Gao H, Liu Z, Dollet L, et al. Disrupted circadian oscillations in type 2 diabetes are linked to altered rhythmic mitochondrial metabolism in skeletal muscle. *Sci Adv*. 2021;7:eabi9654. doi: 10.1126/sciadv.abi9654
  60. Ministro A, de Oliveira P, Nunes RJ, Dos Santos Rocha A, Ferreira T, Goyri-O'Neill J, Rosa Santos SC. Assessing therapeutic angiogenesis in

- a murine model of hindlimb ischemia. *J Vis Exp*. 2019;148:e59582. doi: 10.3791/59582
61. Douma LG, Gumz ML. Circadian clock-mediated regulation of blood pressure. *Free Radic Biol Med*. 2018;119:108–114. doi: 10.1016/j.freeradbiomed.2017.11.024
  62. Pan X, Mota S, Zhang B. Circadian clock regulation on lipid metabolism and metabolic diseases. *Adv Exp Med Biol*. 2020;1276:53–66. doi: 10.1007/978-981-15-6082-8\_5
  63. Hwang JW, Sundar IK, Yao H, Sellix MT, Rahman I. Circadian clock function is disrupted by environmental tobacco/cigarette smoke, leading to lung inflammation and injury via a SIRT1-BMAL1 pathway. *FASEB J*. 2014;28:176–194. doi: 10.1096/fj.13-232629
  64. Takeda N, Maemura K. Circadian clock and the onset of cardiovascular events. *Hypertens Res*. 2016;39:383–390. doi: 10.1038/hr.2016.9
  65. Yang G, Zhang J, Jiang T, Monslow J, Tang SY, Todd L, Pure E, Chen L, FitzGerald GA. Bmal1 deletion in myeloid cells attenuates atherosclerotic lesion development and restrains abdominal aortic aneurysm formation in hyperlipidemic mice. *Arterioscler Thromb Vasc Biol*. 2020;40:1523–1532. doi: 10.1161/ATVBAHA.120.314318
  66. Huo M, Huang Y, Qu D, Zhang H, Wong WT, Chawla A, Huang Y, Tian XY. Myeloid Bmal1 deletion increases monocyte recruitment and worsens atherosclerosis. *FASEB J*. 2017;31:1097–1106. doi: 10.1096/fj.201601030R
  67. Peng X, Fan R, Xie L, Shi X, Dong K, Zhang S, Tao J, Xu W, Ma D, Chen J, et al. A growing link between circadian rhythms, type 2 diabetes mellitus and Alzheimer's disease. *Int J Mol Sci*. 2022;23:504. doi: 10.3390/ijms23010504
  68. Stenvers DJ, Scheer F, Schrauwen P, la Fleur SE, Kalsbeek A. Circadian clocks and insulin resistance. *Nat Rev Endocrinol*. 2019;15:75–89. doi: 10.1038/s41574-018-0122-1
  69. Acosta-Rodríguez VA, Rijo-Ferreira F, Green CB, Takahashi JS. Importance of circadian timing for aging and longevity. *Nat Commun*. 2021;12:2862. doi: 10.1038/s41467-021-22922-6
  70. Duffy JF, Zitting KM, Chinoy ED. Aging and circadian rhythms. *Sleep Med Clin*. 2015;10:423–434. doi: 10.1016/j.jsmc.2015.08.002
  71. Evrard SM, Lecce L, Michelis KC, Nomura-Kitabayashi A, Pandey G, Purushothaman KR, d'Escamard V, Li JR, Hadri L, Fujitani K, et al. Endothelial to mesenchymal transition is common in atherosclerotic lesions and is associated with plaque instability. *Nat Commun*. 2016;7:11853. doi: 10.1038/ncomms11853
  72. Chen PY, Qin L, Baeyens N, Li G, Afolabi T, Budatha M, Tellides G, Schwartz MA, Simons M. Endothelial-to-mesenchymal transition drives atherosclerosis progression. *J Clin Invest*. 2015;125:4514–4528. doi: 10.1172/JCI82719
  73. Tang H, Zhu M, Zhao G, Fu W, Shi Z, Ding Y, Tang X, Guo D. Loss of CLOCK under high glucose upregulates ROCK1-mediated endothelial to mesenchymal transition and aggravates plaque vulnerability. *Atherosclerosis*. 2018;275:58–67. doi: 10.1016/j.atherosclerosis.2018.05.046
  74. Viswambaran H, Carvas JM, Antic V, Marecic A, Jud C, Zaugg CE, Ming XF, Montani JP, Albrecht U, Yang Z. Mutation of the circadian clock gene Per2 alters vascular endothelial function. *Circulation*. 2007;115:2188–2195. doi: 10.1161/CIRCULATIONAHA.106.653303
  75. Obara H, Matsubara K, Kitagawa Y. Acute limb ischemia. *Ann Vasc Dis*. 2018;11:443–448. doi: 10.3400/avd.ra.18-00074
  76. Peek CB. Metabolic implications of circadian-HIF crosstalk. *Trends Endocrinol Metab*. 2020;31:459–468. doi: 10.1016/j.tem.2020.02.008
  77. Deev R, Plaksa I, Bozo I, Isaev A. Results of an international postmarketing surveillance study of pi-VEGF165 safety and efficacy in 210 patients with peripheral arterial disease. *Am J Cardiovasc Drugs*. 2017;17:235–242. doi: 10.1007/s40256-016-0210-3
  78. Deev R, Plaksa I, Bozo I, Mzhavanadze N, Suchkov I, Chervyakov Y, Staroverov I, Kalinin R, Isaev A. Results of 5-year follow-up study in patients with peripheral artery disease treated with PL-VEGF165 for intermittent claudication. *Ther Adv Cardiovasc Dis*. 2018;12:237–246. doi: 10.1177/1753944718786926
  79. Rajagopalan S, Mohler ER 3rd, Lederman RJ, Mendelsohn FO, Saucedo JF, Goldman CK, Blebea J, Macko J, Kessler PD, Rasmussen HS, et al. Regional angiogenesis with vascular endothelial growth factor in peripheral arterial disease: a phase II randomized, double-blind, controlled study of adeno-viral delivery of vascular endothelial growth factor 121 in patients with disabling intermittent claudication. *Circulation*. 2003;108:1933–1938. doi: 10.1161/01.CIR.0000093398.16124.29
  80. McGuigan MR, Bronks R, Newton RU, Sharman MJ, Graham JC, Cody DV, Kraemer WJ. Muscle fiber characteristics in patients with peripheral arterial disease. *Med Sci Sports Exerc*. 2001;33:2016–2021. doi: 10.1097/00005768-200112000-00007
  81. Mitchell RG, Duscha BD, Robbins JL, Redfern SI, Chung J, Bensimhon DR, Kraus WE, Hiatt WR, Regensteiner JG, Annex BH. Increased levels of apoptosis in gastrocnemius skeletal muscle in patients with peripheral arterial disease. *Vasc Med*. 2007;12:285–290. doi: 10.1177/1358863X07084858
  82. Koutakis P, Weiss DJ, Miserlis D, Shostrom VK, Papoutsi E, Ha DM, Carpenter LA, McComb RD, Casale GP, Pipinos II. Oxidative damage in the gastrocnemius of patients with peripheral artery disease is myofiber type selective. *Redox Biol*. 2014;2:921–928. doi: 10.1016/j.redox.2014.07.002
  83. Amthor H, Macharia R, Navarrete R, Schuelke M, Brown SC, Otto A, Voit T, Muntoni F, Vrbova G, Partridge T, et al. Lack of myostatin results in excessive muscle growth but impaired force generation. *Proc Natl Acad Sci USA*. 2007;104:1835–1840. doi: 10.1073/pnas.0604893104
  84. Elkasrawy MN, Hamrick MW. Myostatin (GDF-8) as a key factor linking muscle mass and bone structure. *J Musculoskelet Neuronal Interact*. 2010;10:56–63.
  85. Schroder EA, Harfmann BD, Zhang X, Srikuea R, England JH, Hodge BA, Wen Y, Riley LA, Yu Q, Christie A, et al. Intrinsic muscle clock is necessary for musculoskeletal health. *J Physiol*. 2015;593:5387–5404. doi: 10.1113/JP271436
  86. Hennebery A, Berry C, Siriott V, O'Callaghan P, Chau L, Watson T, Sharma M, Kambadur R. Myostatin regulates fiber-type composition of skeletal muscle by regulating MEF2 and MyoD gene expression. *Am J Physiol Cell Physiol*. 2009;296:C525–C534. doi: 10.1152/ajpcell.00259.2007
  87. Grade CVC, Mantovani CS, Alvares LE. Myostatin gene promoter: structure, conservation and importance as a target for muscle modulation. *J Anim Sci Biotechnol*. 2019;10:32. doi: 10.1186/s40104-019-0338-5
  88. Tsimakouridze EV, Alibhai FJ, Martino TA. Therapeutic applications of circadian rhythms for the cardiovascular system. *Front Pharmacol*. 2015;6:77. doi: 10.3389/fphar.2015.00077
  89. Bonten TN, Saris A, van Oostrom MJ, Snoep JD, Rosendaal FR, Zwaginga J, Eikenboom J, van der Meer PF, van der Bom JG. Effect of aspirin intake at bedtime versus on awakening on circadian rhythm of platelet reactivity. A randomized cross-over trial. *Thromb Haemost*. 2014;112:1209–1218. doi: 10.1160/TH14-05-0453
  90. Manfredini R, Gallerani M, Portaluppi F, Salmi R, Zamboni P, Fersini C. Circadian variation in the onset of acute critical limb ischemia. *Thromb Res*. 1998;92:163–169. doi: 10.1016/s0049-3848(98)00127-3
  91. Smolensky MH, Portaluppi F, Manfredini R, Hermida RC, Tiseo R, Sackett-Lundeen LL, Haus EL. Diurnal and twenty-four hour patterning of human diseases: cardiac, vascular, and respiratory diseases, conditions, and syndromes. *Sleep Med Rev*. 2015;21:3–11. doi: 10.1016/j.jsmrv.2014.07.001
  92. Amstrup AK, Sikjaer T, Pedersen SB, Heickendorff L, Mosekilde L, Rejnmark L. Reduced fat mass and increased lean mass in response to 1 year of melatonin treatment in postmenopausal women: a randomized placebo-controlled trial. *Clin Endocrinol (Oxf)*. 2016;84:342–347. doi: 10.1111/cen.12942
  93. Garfinkel D, Zorin M, Wainstein J, Matas Z, Laudon M, Zisapel N. Efficacy and safety of prolonged-release melatonin in insomnia patients with diabetes: a randomized, double-blind, crossover study. *Diabetes Metab Syndr Obes*. 2011;4:307–313. doi: 10.2147/DMSO.S23904
  94. Potter GD, Skene DJ, Arendt J, Cade JE, Grant PJ, Hardie LJ. Circadian rhythm and sleep disruption: causes, metabolic consequences, and countermeasures. *Endocr Rev*. 2016;37:584–608. doi: 10.1210/er.2016-1083
  95. Gabriel BM, Zierath JR. Circadian rhythms and exercise - re-setting the clock in metabolic disease. *Nat Rev Endocrinol*. 2019;15:197–206. doi: 10.1038/s41574-018-0150-x
  96. Saratzis A, Paraskevopoulos I, Patel S, Donati T, Biasi L, Diamantopoulos A, Zayed H, Katsanos K. Supervised exercise therapy and revascularization for intermittent claudication: network meta-analysis of randomized controlled trials. *JACC Cardiovasc Interv*. 2019;12:1125–1136. doi: 10.1016/j.jcin.2019.02.018
  97. Treat-Jacobson D, McDermott MM, Beckman JA, Burt MA, Creager MA, Ehrman JK, Gardner AW, Mays RJ, Regensteiner JG, Salisbury DL, et al; American Heart Association Council on Peripheral Vascular Disease; Council on Cardiovascular and Stroke Nursing; Council on Epidemiology and Prevention; and Council on Lifestyle and Cardiometabolic Health. Implementation of supervised exercise therapy for patients with symptomatic peripheral artery disease: a science advisory from the American Heart Association. *Circulation*. 2019;140:e700–e710. doi: 10.1161/CIR.0000000000000727
  98. Norgren L, Weiss N, Nikol S, Lantis JC, Patel MR, Hincliffe RJ, Reinecke H, Volk HD, Reinke P, Fadini GP, et al. PACE: randomized, controlled, multicentre, multinational, phase III study of PLX-PAD for critical limb ischaemia in patients unsuitable for revascularization: randomized clinical trial. *Br J Surg*. 2024;111:znad437. doi: 10.1093/bjs/znad437
  99. Ruan W, Yuan X, Eltzschig HK. Circadian rhythm as a therapeutic target. *Nat Rev Drug Discov*. 2021;20:287–307. doi: 10.1038/s41573-020-00109-w